nature communications

Article

https://doi.org/10.1038/s41467-025-65073-8

Unlocking vehicle-to-grid potential of load shifting in China's megacities considering comprehensive real-world behaviors

Received: 3 December 2024

Accepted: 7 October 2025

Published online: 18 November 2025

Check for updates

Kaisan Li[1], Xinxin Li[1], Zuxun Xiong[2], Shengyu Tao[1], Gucheng Zhao[1], Yi Jiang[1,3], He Qi[4] & Yi Zhang[1]

Global decarbonization necessitates large-scale electrification, bringing load stability challenges to urban grids. While Vehicle-to-grid (V2G) technology using private plug-in electric vehicles (P-PEVs) can balance the loads, its potential at megacity-level remains unclear due to the complexity of fine-grained, user-centric modelling. Here, we propose a Mobility and V2G Coupled (MOVC) framework, which depicts individual P-PEV travel-charge behaviors and evaluates user V2G concerns regarding willingness, compensation, and battery degradation. The framework analyzes 480,000 P-PEVs in Shenzhen, China, revealing a 2300 MW peak-shaving capacity, reducing peak-valley ratios by 73%. V2G strategies that prioritize user satisfaction hardly sacrifice the load shifting performance, but reduce battery degradation costs and compensation costs by 30-40% and 5-13% respectively. A forward-looking scenario considering fully-deployed quick charging (QC) in four China's megacities reveals 0%-12% lower peak-valley ratios with more inequal V2G scheduling (4%-95% higher standard deviation). This study enlightens megacity-level V2G potential evaluations and their policy-making considering real-world behaviors.

China's 2020 commitment to achieve carbon peak by 2030 and neutrality by 2060 aligns with its rapid electrification roadmap, targeting 64% industrial electrification by 2050 to transition from fossil fuel dependence toward sustainable energy[1–3]. However, the foreseeable widespread adoption of electric equipment challenges urban distribution grids, requiring techniques, e.g., load shifting, to stabilize voltage levels and improve efficiency[4]. While immobile batteries enable load shifting, their centralized deployment raises considerable safety concerns, shifting research focus to dispatch distributed private plug-in electric vehicles (P-PEVs) and their onboard batteries with controllable battery safety and recycling solutions[5–10]. This vision is supported by Vehicle-to-grid (V2G) technology, which is extensively explored to have noticeable benefits in load shifting[11–13], energy savings[14–17], and economic gains[15,18–21]. China's rapidly expanding P-PEV market further broadens the operational potential of V2G, making it promising to utilize the onboard batteries for urban load shifting via V2G without sacrificing their mobility demand[22–24].

However, making city-level decisions on V2G policies and incentives is difficult without reliable quantitative analysis.

Existing literature mainly considers V2G based on the mobility or charging behavior of PEVs. The mobility models are proposed to distinguish the spatial movement patterns of individuals. Those methods can be divided into Origin-destination (OD) analysis[25–27], Markov Chain-based models[28–30], OD-based trip chain models[31–33], graph-based models[34], etc. The charging models include more subdivisions, covering large-scale valley filling[35,36], load forecasting[37], user-oriented charging behavior analysis and scheduling strategies[38–41], V2G arbitrage[42,43], user willingness of participating V2G and incentive mechanisms[44–52], range anxiety[53], battery degradation effects[54–58], V2G optimization relaxation[59–61], etc. Multiple methodologies are leveraged

[1]Tsinghua Shenzhen International Graduate School, Tsinghua University, Shenzhen, China. [2]Department of Engineering Science, University of Oxford, Oxford, UK. [3]Department of Building Science, School of Architecture, Tsinghua University, Beijing, China. [4]China Construction Science and Technology Group Co. Ltd, Beijing, China. e-mail: zy1214@sz.tsinghua.edu.cn

to address these problems with high accuracy or efficiency, including mixed-integer linear programming[43,53], heuristic algorithms[41,42,62], stochastic programming[46,47,57], deep reinforcement learning[63–65], user surveys[44,48,49,51], simulations[54,58], experimental measurements[55], etc. However, existing works have their scopes narrowed in single or several subareas by studying basically microgrids or small PEV fleets, with megacity-level user behaviors being considerably underinvestigated. This noticeable gap is critically prohibitive for megacity policymakers to consider V2G promotion and their sustainable integration into many energy infrastructures.

A noteworthy research branch lies in integrating the mobility and charging patterns of PEVs to reveal spatial-temporal V2G insights from large-scale real-world data observations. The related works can be divided into local viewpoints and global ones. For the former, Bian et al. discuss the time-space distribution of PEVs within a given distribution grid[62]. Wu et al. propose a V2G scheduling method considering home, work and commercial microgrids[66]. Orfanoudakis et al. present a V2G simulation platform, which considers various user traveling behaviors in public, work and residential places, and evaluates user V2G satisfaction and battery degradation[67]. However, these works mainly adopt a grid operator-centric perspective, where the user traveling features are simplified to entries and exits within predefined regions. For the latter, Zhang et al. analyze V2G implementation potential across Japan's prefectures, considering regional differences in power demand, temperature, user behavior, etc[68]. Xu et al. integrate large-scale mobile phone data and PEV charging profiles to estimate fine-grained PEV mobility and energy demand[69]. Qian et al. develop a simulation platform to discuss V2G operations in coupled urban power and transportation networks[70]. Zhang et al. combine travel patterns and charging behaviors to predict EV charging demand in Beijing[71]. However, since the computational costs increase significantly with the growth of PEV scale, the scopes of these works are reduced in terms of either tasks (coordinated charging[69], load forecasting[71–73]) or modeling details (regional transportation networks[70], simplified charging costs[70] or charging behaviors[68]). However, systematic evaluations of V2G potential at the megacity level have been limited, largely due to unresolved challenges in fine-grained modeling considering user-centric private user behavior patterns.

In this paper, we present a Mobility and V2G Coupled (MOVC) framework for systematic, megacity-scale evaluation of V2G potential. Figure 1a and Fig. 1b give an overview of the research methodology. The framework comprehensively considers various V2G factors among hundreds of thousands of P-PEVs, including vehicle traveling-charging behaviors, user willingness and incentives, range anxiety, and battery

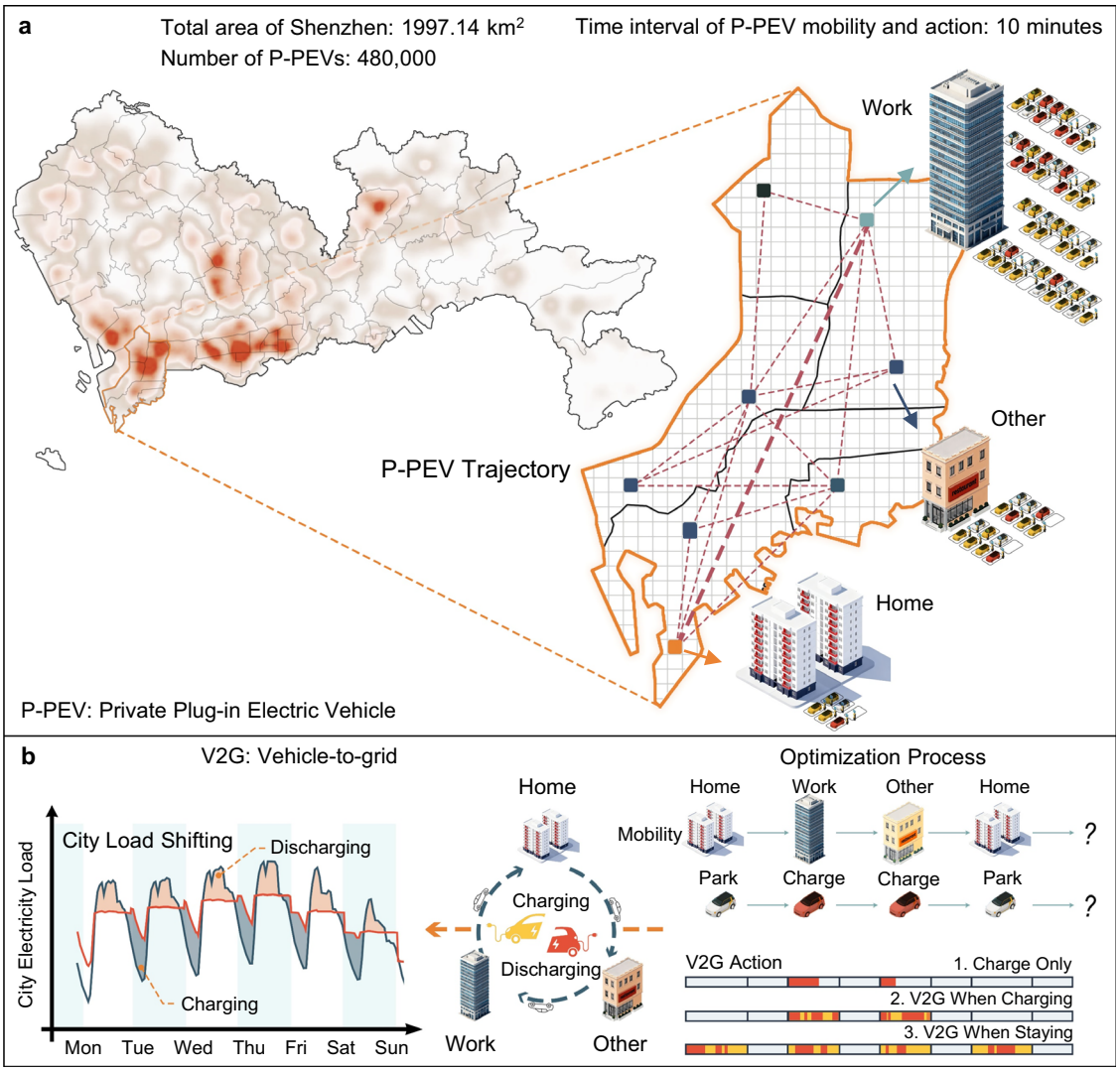

Fig. 1 | Coupling P-PEV mobility and V2G behavior for urban load balancing. **a** Extracting P-PEV trajectories from massive travel records. We discretize the area of Shenzhen into meshed stay regions and mark them as Home, Work, and Other places for each P-PEV user. **b** The charging framework for simulating the users' charging decisions upon their stay actions. An optimization model is introduced to schedule the V2G events among P-PEVs. Various extents of V2G participation represent distinct patterns of P-PEV power flows, which will be leveraged for peak shaving and valley filling of the overall load of Shenzhen.

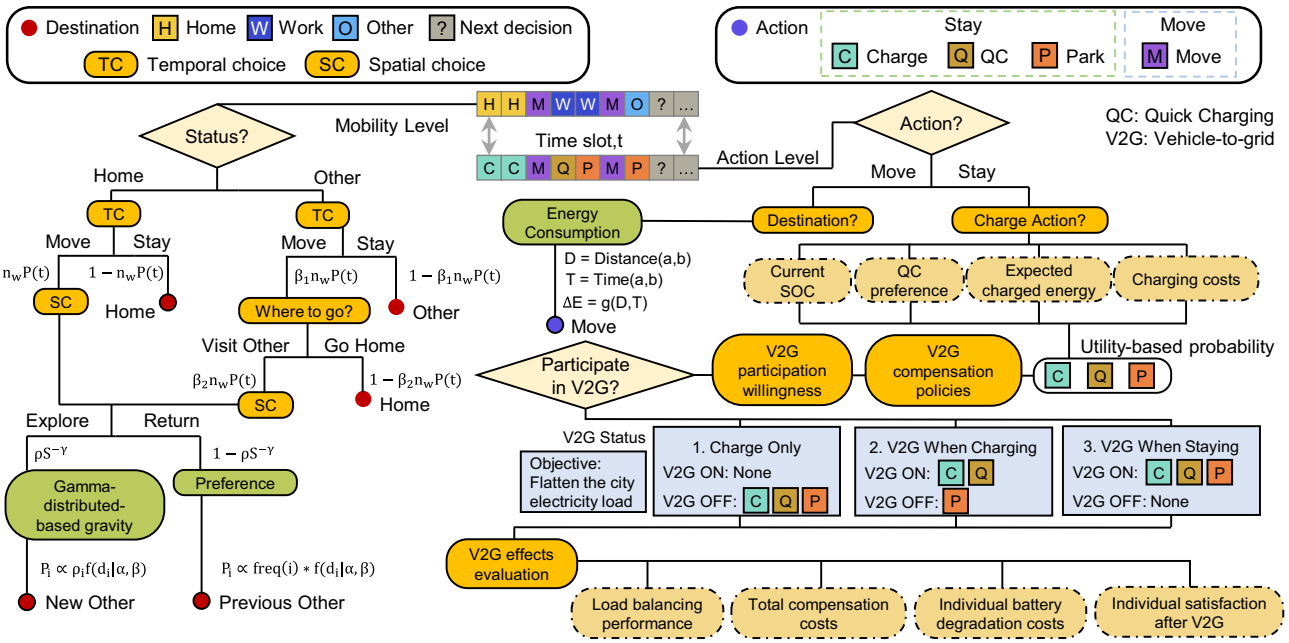

Fig. 2 | An overview of the MOVC framework. The MOVC framework assigns mobility and charging information for each time slot. In the Timegeo[28]-based mobility model, temporal choices of PEVs are controlled by user-specific parameters, including home-based hours (n_w), dwell rate (β_1), and burst rate (β_2). Spatial choices are made by combining the gravity model[79] and the gamma-distributed-based EPR mechanisms. In the charging model, charging decisions are simulated via utility functions of multiple factors[39]. A compensation mechanism[46] is utilized to simulate users' participation in three different V2G strategies. The objective is designed to flatten the city's electricity load as much as possible. The effects of V2G are evaluated considering load balancing performance, total compensation costs[46], battery degradation costs[56] and users' satisfaction after V2G[67]. Energy consumption during movement is estimated based on travel distance and travel time[74].

degradation costs. The above considerations are derived from a user-centric perspective, capable of depicting traveling patterns and multi-dimensional energy dispatching effects of every individual. The framework illustrates V2G potential in Shenzhen and other three China's megacities, considering seasonal load variations, growing P-PEV penetration rates, discrepancies of traveling characteristics in different cities, and quick charging (QC) availability. Specifically, we follow the settings of Timegeo[28] to simulate travel patterns of P-PEVs in Shenzhen and Beijing based on 9,108,081 and 9,651,948 location records from 36,932 and 38,129 anonymous P-PEV users, respectively. The number of P-PEVs is further expanded to 480,000 or larger to match the holdings of the cities. To model charging actions, we modify the utility-based model[39] to consider possible inclination to range anxiety mitigation, larger charging power and lower charging costs among users. We implement large-scale V2G optimization via a linear-programming (LP)-based model with proper relaxations[59–61] to flatten the city load curve as much as possible under different constraints. Our results indicate that fully utilizing the parking time of collective P-PEVs for V2G can release 2332 and 2320 MW of peak shaving and valley filling capacity during annual peak hours in Shenzhen. The weekly median peak-valley difference ratio (PVDR) can be accordingly reduced from 0.362 to 0.097. Adjusting V2G strategies to maintain higher user V2G satisfaction may reduce 30–40% battery degradation costs and 5–13% V2G compensation costs. In the assumed future with higher P-PEV penetration rates and upgraded residential distribution grids to support QC, our results indicate marginal additional V2G benefits but more inequal energy scheduling among users.

Results

Mobility and vehicle-to-grid coupled model

This study utilizes multiple real-world datasets, including (1) 2022 Shenzhen P-PEV Trajectories Dataset (2022 SPTD) and 2022 Beijing P-PEV Trajectories Dataset (2022 BPTD), which collect three-month 9,108,081 and 9,651,948 location records of 36,932 and 38,129 anonymous P-PEV users in Shenzhen and Beijing, respectively. (2) 2019 Shenzhen Parking Census Dataset (2019 SPCD), which contains 9748 parking lots with information on geographical positions and parking spot capacity. (3) 2019 National PEV Big Data Statistics (2019 NPBDS), which extracts distributions of PEV daily average travel distance and monthly average charging time. (4) 2019 Shenzhen electricity load profile, which gives the overall load of the city. We expand the number of P-PEVs to 480,000 to match the actual holdings of Shenzhen in 2022 (see Supplementary Note. 1).

We develop the MOVC framework for fine-scale estimation of P-PEV mobility and charging patterns (see Fig. 2). For mobility modeling, we divide the stay regions of P-PEVs into Home, Work and Other. Following the basic paradigm of Timegeo[28], users make temporal and spatial choices probabilistically according to their located regions and user-specific traveling parameters (see Methods, Supplementary Figs. 1,3,4b,6, and Supplementary Note. 1). For charging modeling, we consider all possible actions of P-PEVs as (1) Move, where the vehicles travel in the city. (2) Park, where users intend to park the vehicles without plugging chargers in them. (3) Charge, where users park the vehicles and plug the slow chargers into their slow charging sockets. (4) QC, where users park the vehicles and plug the QC chargers into their QC sockets. The latter three cases are summarized by the term "Stay" to represent a general situation where P-PEVs are immobile. Energy consumption during Move is calculated by the drivetrain losses[74] (see Methods). If a vehicle is in a Stay, MOVE uses a utility-based model[39] to specify its action of Park, Charge, or QC. The decisions are affected by multiple realistic factors, e.g., the vehicle's current state of charge (SOC), the user's preference towards QC, the expected energy that can be obtained in the Stay, depending on Stay duration, along with available charging modes, and charging costs depending on the current time period and location (public or private). One can refer to Methods for details. Notably, we assume that all the decisions of Park, Charge and QC are made upon the arrival of Stay-s. Next, MOVC simulates P-PEVs' participation in V2G by considering

https://doi.org/10.1038/s41467-025-65073-8

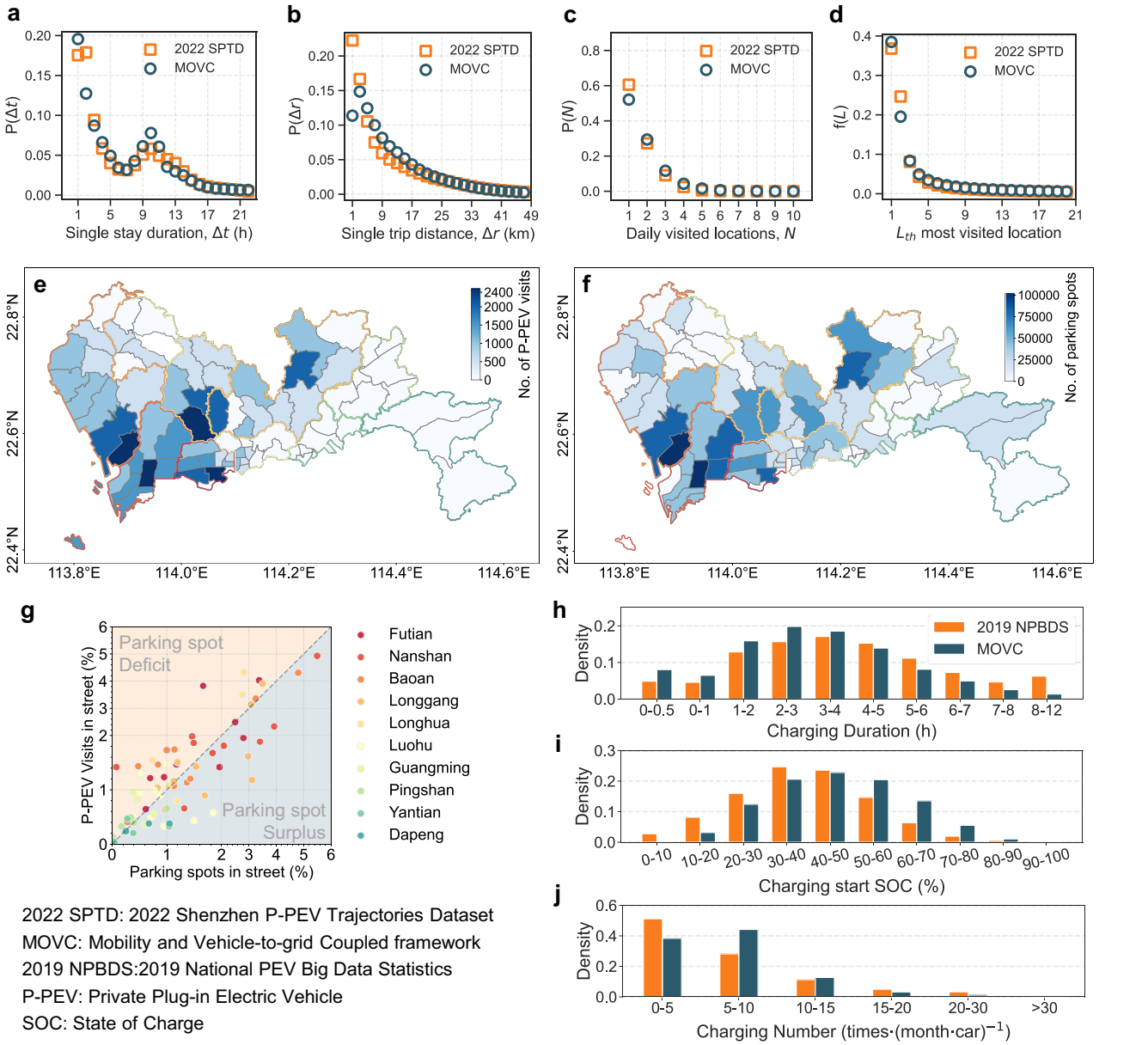

Fig. 3 | Validation of the MOVC framework in mobility and charging behavior. **a**–**d** Probability distributions of single stay duration, single trip distance, number of daily visited locations, and visiting the Lth most visited location. We compare the results of MOVC with the 2022 SPTD. **e**, **f** Spatial distributions of parking spot numbers (from 2019 SPCD) and visit numbers (from 2022 SPTD) in Shenzhen. **g** Comparison between the number of parking spots and the one of visits, decomposed into each district in Shenzhen. **h**–**j** Probability distributions of charging start SOC, charging duration, and monthly charging number, of MOVC results and 2019 NPBDS.

economic subsidies. The compensations required for obeying V2G scheduling are modeled as normal distributions[46]. Given a specific compensation rate γ, users will decide which V2G scenario to join depending on whether their expected economic gains are met (see Methods and Supplementary Fig. 9). We design three scenarios, namely (1) Charge Only, where V2G is disabled and only unidirectional energy flows from the power grid to the vehicles, (2) V2G When Charging (VWC), where V2G is enabled in Charge and QC actions, and (3) V2G When Staying (VWS), where users are required to plug the chargers in their vehicles to enable V2G once they are in Stay. In other words, VWS compulsorily switches the vehicles' states in Park from isolated to connected (to the grid). Accordingly, users who participated in VWS will receive higher compensation compared to those in VWC. Finally, the V2G effects are evaluated in four aspects, namely (1) load balancing performance, (2) total compensation costs paid to users involved in V2G, (3) individual battery degradation costs, and (4) individual satisfaction after V2G activities. The above metrics are designed to comprehensively assess V2G outcomes in city power stabilization, economic input, and widely concerned V2G impacts on batteries and range anxiety.

The simulation results of MOVC are verified with real-world datasets. For the mobility model, we compare several key characteristics, namely (1) single stay duration, describing the distribution of duration of each Stay, (2) single trip distance, giving the distribution of traveling distance of each Move, (3) number of daily visited locations, and (4) the Lth most visited locations, denoting the frequency of all P-PEV users visiting their 1-st, 2-nd, 3-rd, …, Lth most visited locations, as explained in details in Supplementary Note. 1 and Supplementary Table. 2. The respective results in Fig. 3a–d exhibit good agreement. We compare the identified Home labels of P-PEVs with the distribution

of parking spots in Shenzhen, according to the 2019 SPCD (Fig. 3e–g). The similar distributions of parking spots and Home labels support us to expand the number of P-PEVs from 36,932 to larger values according to the proportions of street-level parking spots, as explained in Supplementary Note. 1. For the charging model, we simulate the charging behaviors in a base case, which will be further discussed in the following sections. We compare the distributions of charging start SOC, charging duration and monthly charging times under the base case with the ones given by the 2019 NPBDS, as shown in Fig. 3h–j.

Illustration of Shenzhen private plug-in electric vehicle load profile under Charge Only

Charge Only represents a general real-world situation where V2G planning is not introduced, and P-PEV users charge their vehicles disorderly according to their own energy demand. We hence set up a base case under Charge Only to reflect the temporal-spatial load characteristics with disordered P-PEV energy usage patterns. The details of the base case can be found in Supplementary Table 5. For spatial distributions, we illustrate the weekly peak load and the number of charging events of all stay regions in Fig. 4a, along with a district-level decomposition in Fig. 4b. The weekly peak mainly concentrates on Yuehai Street (Nanshan), Bantian Street (Longgang), and Futian Street (Futian). The former two are the most economically active areas in Shenzhen, housing prominent companies, e.g., Tencent, Huawei and China Resources, while the latter holds Futian and Huanggang ports as transportation hubs between Shenzhen and Hong Kong. Additionally, the Luohu district has a noticeable aggregated peak load, although its stay-region-level peak values are relatively intermediate.

We then decompose the P-PEV charging load into charging places (Home, Work, Other) and districts, as shown in Fig. 4c. Considering the time-of-use (ToU) electricity price, charging between 0 AM and 8 AM yields the lowest costs. Also, charging at private places (Home) is cheaper than at public places (Work, Other) by 0.6 RMB (around 0.083 USD) per kWh[75]. Both factors make Home charging dominate, especially at midnight, pushing the peak value to 375.18 MW. However, compared with Shenzhen's electricity load in different seasons, the load of P-PEVs accounts for only 2% in general, indicating that the given P-PEV penetration rate will not significantly burden the power grid. From the perspective of city load fluctuation, the grid may even benefit since the city valley load and the P-PEV charging peak load coincide at midnight under the guidance of ToU, a valley-filling effect can thus be expected.

Additionally, we demonstrate the dispatchable potential of city-scale collective P-PEV batteries in Fig. 4d. For each P-PEV, we define Charge Potential as the maximum amount of energy it can charge during a stay and Discharge Potential as the maximum amount of energy it can discharge likewise. Additionally, Capacity Limit represents the battery's maximum capacity, and SOC Demand indicates the energy required to support trips occurring in the next 24 h. Considering the constraint of limited Stay duration, either Charge Potential or Discharge Potential cannot strictly reach the upper or lower limit. Detailed computation is given in Methods. Charge Only determines the collective current capacity in the yellow full line, with an average of 18186.77 MWh. As a contrast, the average values of Charge Potential and Discharge Potential are 26227.23 MWh and 4789.94 MWh, respectively. Therefore, a possible variation of the current capacity (yellow dashed line) may be realized via V2G scheduling for city load balancing, indicating that a significant portion of P-PEV energy storage resources remains underexploited. Note that Fig. 4d only gives a schematic diagram, which may differ from actual constraints considered in the V2G optimization. The reasons are given in Supplementary Fig. 8.

Case analysis of Shenzhen private plug-in electric vehicle load profile variations under Charge Only

The base case discussed above considers users' charging concerns relatively evenly. In this section, we design several cases to demonstrate the possible variations of P-PEV load profiles with different intensities of QC preference, range anxiety and sensitivity of charging costs. Specifically, we assume (1) Case 1, where users are very sensitive to a decrease in the SOC, and the charging probability quickly increases when the SOC levels go lower[39]. (2) Case 2, where users are not sensitive to SOC levels unless the SOC reaches a threshold[39]. (3) Case 3, where users prefer larger charging power and tend to choose QC. (4) Case 4, where a public charging subsidy policy is introduced, and charging at Home yields identical costs compared with charging at Work, Other. (5) Case 5, where the factor of charging costs has no effect on users' charging decisions. The parameter settings of all cases are given in Supplementary Table. 5. Note that in all cases, we assume that QC is only available at Work, Other, since most of the residential areas in China do not allow QC due to limited capacities of the distribution grid.

As shown in Fig. 5a, Base case, Case 1 and Case 2 have similar load patterns concentrated at midnight. In Fig. 5b, a daytime peak appears in Case 3, reflecting users' tendency towards QC at public places. In Fig. 5c, since public charging is subsidized in Case 4, the daytime peak further turns to a daily peak since Home charging is not attractive in terms of costs. The phenomenon will push the city's peak load higher since the latter also appears in daytime. Case 5 generates double-peak patterns at midnight and morning, the peak value becomes mild while the daytime load is generally higher than the Base case, Case 1 and Case 2.

We compare the number of charging events under different cases in Fig. 5e. Case 1 generates significantly more charging events due to severe range anxiety. In contrast, Case 2 only keeps necessary charging activities. In Case 3, where users prefer larger power, the proportion of QC in public places is increased noticeably. In Cases 4 and 5, Work charging occurs more frequently compared with the Base case, and Other charging begins to dominate.

We illustrate the proportion of duration of all actions (Move, Park, Charge, QC) under different cases in Fig. 5f. In all cases, the proportion of Park accounts for more than 80% of all actions. Therefore, VWS is expected to utilize the Stay duration much more than VWC for V2G scheduling. The V2G effects of VWC and VWS will be further discussed in the following section.

Vehicle-to-grid optimization considering variations of seasonal load and compensation intensities

In this section, we discuss how distinct compensation policies influence user participation in various V2G programs and how the proposed V2G strategies stabilize city electrical loads across different seasons with varying levels of fluctuation. For the former, we set up four compensation rates $\gamma = 0.5, 1.0, 1.5, 2.0$. Considering the discrepancy of participation duration between VWC and VWS, unit discharge compensation is set as 0.015, 0.03, 0.045, 0.06 RMB (around 0.002-0.008 USD) per kWh and 0.075, 0.15, 0.225, 0.3 RMB (around 0.01–0.04 USD) per kWh, respectively. It should be noted that these values represent only the policy-based V2G subsidies and do not include users' revenue from discharging via feed-in tariffs. The specific participation mechanism is given in Methods and Supplementary Fig. 9. For the latter, we select 4 weeks from the 2019 Shenzhen electricity load profile to represent typical urban loads at all seasons (see Supplementary Fig. 10). The selected summer load contains an annual peak of 19,219 MW, and the fall load has the median weekly peak observed throughout all weeks in 2019. The spring load has a comparable peak to the fall one but exhibits a greater peak-valley difference. The winter load represents an overall lower power demand. The city load fluctuation is evaluated via PVDR, defined as $PV = \frac{L_p - L_v}{L_v}$, where L_p and L_v represent peak load and valley load, respectively.

First, we demonstrate the city load curves under different compensation intensities in Fig. 6. The given curves reflect the combined effects of both VWC- and VWS-involved vehicles. However, since the

https://doi.org/10.1038/s41467-025-65073-8

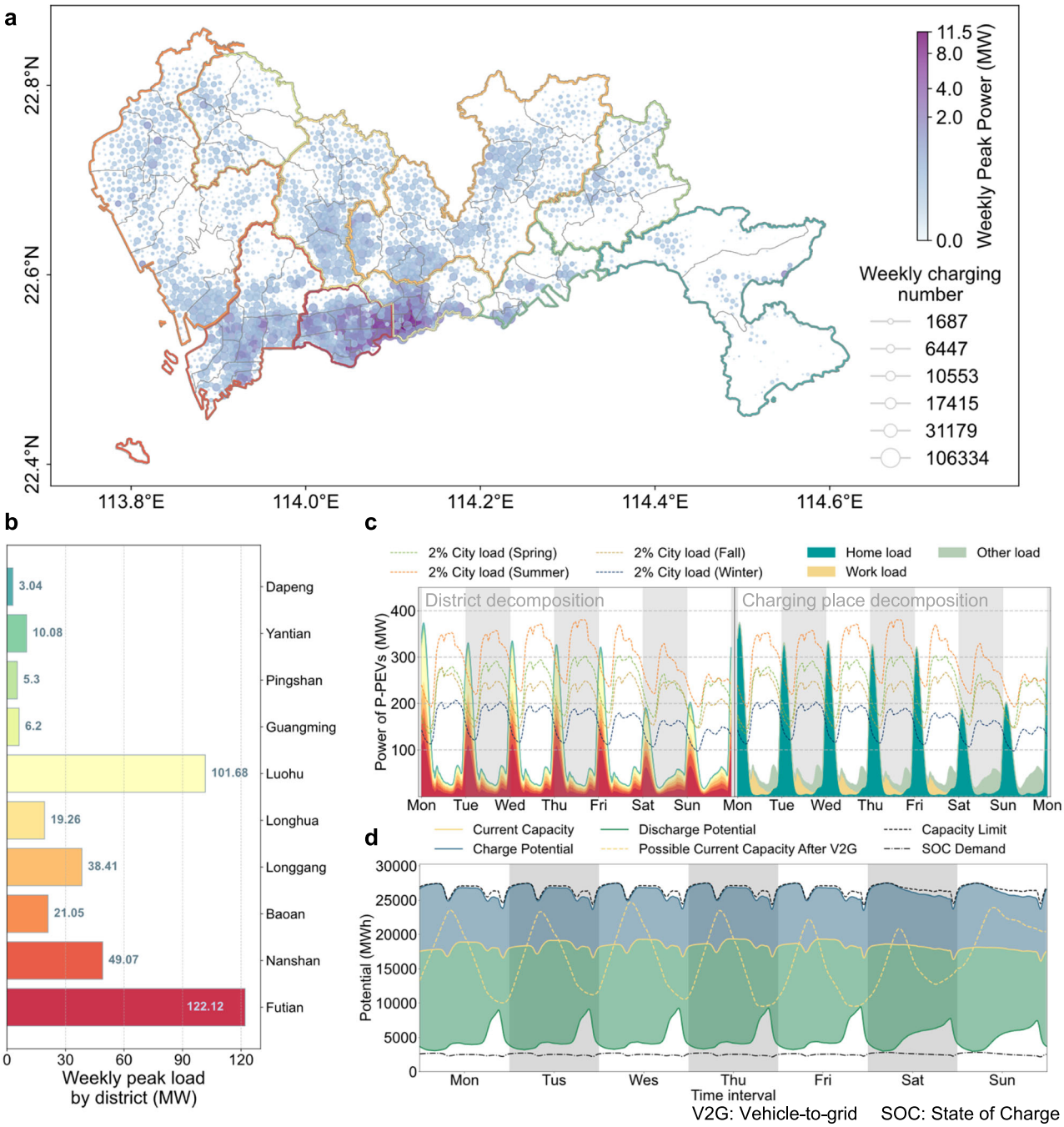

Fig. 4 | Shenzhen P-PEV charging profiles and energy storage potential. **a** Weekly peak load distribution of P-PEVs in Shenzhen, divided into stay regions. **b** Weekly peak load distributions of P-PEVs, divided into districts. **c** The load curve of Shenzhen P-PEVs, divided into charging places (left) and districts (right), respectively. The load magnitude of P-PEVs is comparable to 2% of Shenzhen's electricity peak load. **d** The weekly curve of the current capacity of all P-PEVs, and the maximum (Charge Potential, blue area) or minimum (Discharge Potential, green area) energy that can be achieved by all P-PEVs charging or discharging as much as possible. The two levels are constrained by the total battery capacity (Capacity Limit) and the SOC required for traveling (SOC Demand). The yellow dotted line represents a possible variation of the current capacity curve after V2G scheduling.

V2G effects of VWC are trivial, we illustrate the fitted relationship between PVDR and the number of P-PEVs in VWS in the right boxplots. With the increase of compensation intensity, the weekly median of the city load PVDR gradually decreases from 0.428, 0.362, 0.408, 0.396 to 0.118, 0.097, 0.058, 0.005 at all seasons, respectively. Additionally, the results indicate that every 100,000 P-PEVs participating in VWS scheduling is expected to mitigate the median city load PVDR by 0.06–0.08, accounting for 16.36–20.20% of the metric of original loads.

Next, we further discuss the comparison of several important characteristics between VWC and VWS, including participation scale, peak-shaving and valley-filling effects, battery degradation costs, user satisfaction and total compensation costs. The numbers of P-PEVs involved in two V2G scenarios are provided in Fig. 7a. The differential impacts of varying participation scales in VWC and VWS scenarios on city weekly load peak shaving and valley filling effects are shown in Fig. 7b, c. As previously discussed, VWC exhibits very limited load-balancing potential since it cannot schedule the substantial duration of

https://doi.org/10.1038/s41467-025-65073-8

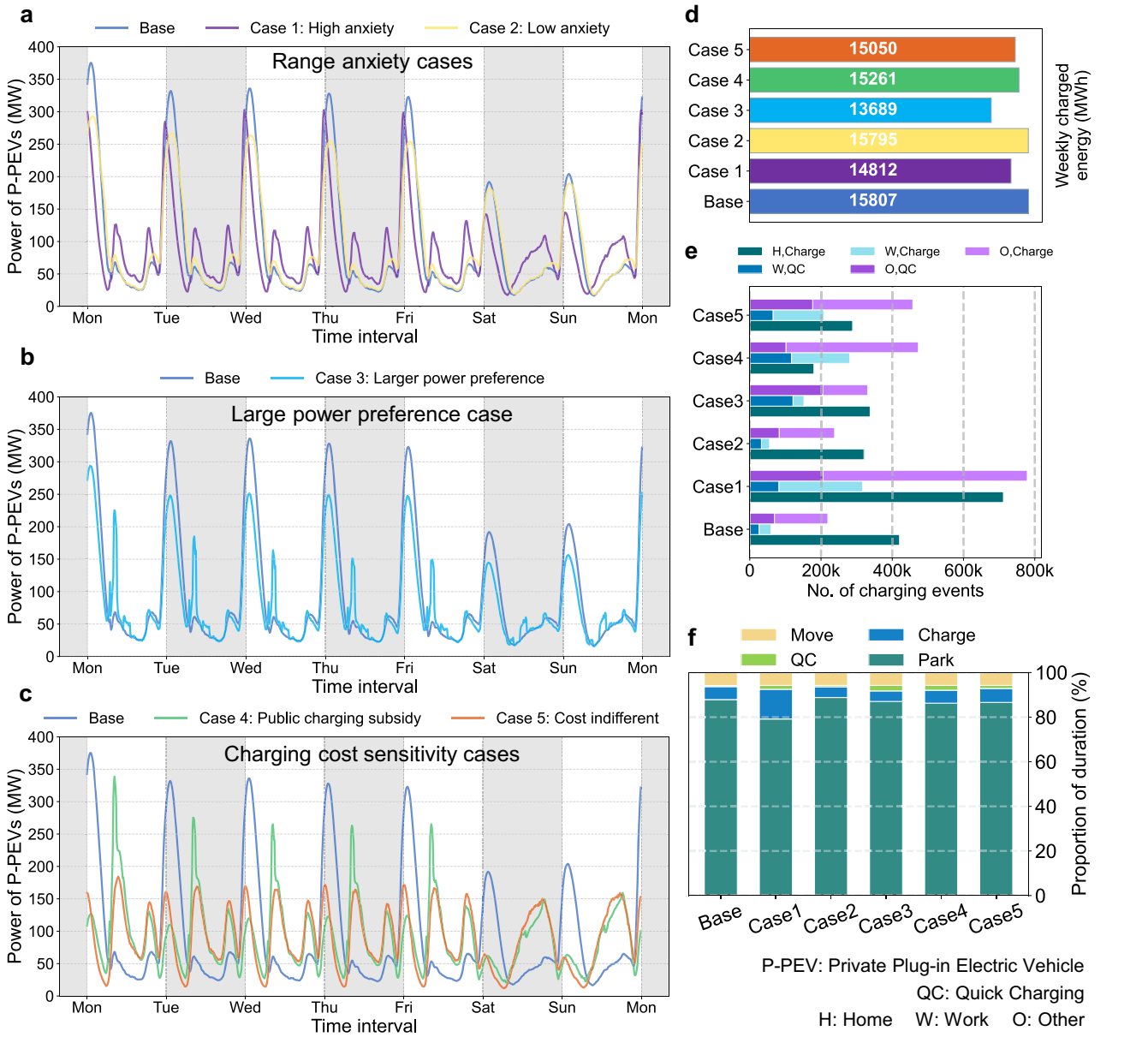

Fig. 5 | P-PEV load profiles under different charging cases. a–c Weekly load curves of P-PEVs under different charging cases and the corresponding values of weekly charged energy. **d** The values of weekly charged energy under different cases. **e** The numbers of Charge and QC events occurring at Home, Work and Other under different cases. **f** Proportions of duration of all possible P-PEV actions (Move, Charge, QC, Park) under different cases.

Park actions. Typically, VWC achieves weekly peak shaving below 10 MW and valley filling under 80 MW. Considering that ToU inherently guides the Charge Only load to off-peak periods, the operational value of VWC is further impaired. In contrast, VWS enables full scheduling flexibility of Park duration and demonstrates pronounced load balancing efficacy, achieving peak shaving of 1330–2332 MW and valley filling of 1475–2320 MW under maximum compensation. Figure 7e illustrates the distributions of individual weekly discharged energy, where the average and median values of VWC reach 6.70–8.98 kWh and 0 kWh, and the metrics of VWS reach 212.42, 213.19, 198.51, 131.66 kWh and 220.19, 220.29, 206.76, 133.84 kWh, respectively. Figure 7f gives distributions of battery degradation costs[56], where the average and median costs of VWC locate between 2.95 and 3.22 RMB (around 0.41–0.44 USD) per week and 2.22–2.32 RMB (around 0.31–0.32 USD) per week, and the values of VWS reach 31.15, 29.41, 25.37, 15.72 RMB (around 4.30–2.17 USD) per week and 31.82, 29.95, 26.30, 16.20 RMB (around 4.39–2.23 USD) per week, respectively. Regarding users' satisfaction after V2G activities[67] shown in Fig. 7g, the median values of VWC generally exceed 80%, while the metrics of VWS are inferior, reaching 50.73%, 47.81%, 67.03%, and 87.30%, respectively. As important indicators of economic compromise, the values of total compensation costs[46] paid to P-PEV users are illustrated in Fig. 7d. Full investment ($\gamma = 2.0$) requires costs of 18.71M–30.29 M RMB (around 2.58M–4.18 M USD) per week. The compensation costs exhibit diminishing marginal returns, where approximately 25% of maximum investment yields peak shaving of 770–1196 MW and valley filling of 925–1195 MW, while 66% investment achieves 1172–2008 MW and 1475–1998 MW, respectively, approaching the performance plateau observed at full investment.

Vehicle-to-grid scheduling considering higher user satisfaction

As discussed above, while VWS demonstrates superior load-balancing performance, this comes at non-trivial economic costs. Furthermore, user satisfaction with V2G dispatching remains low across all seasons

https://doi.org/10.1038/s41467-025-65073-8

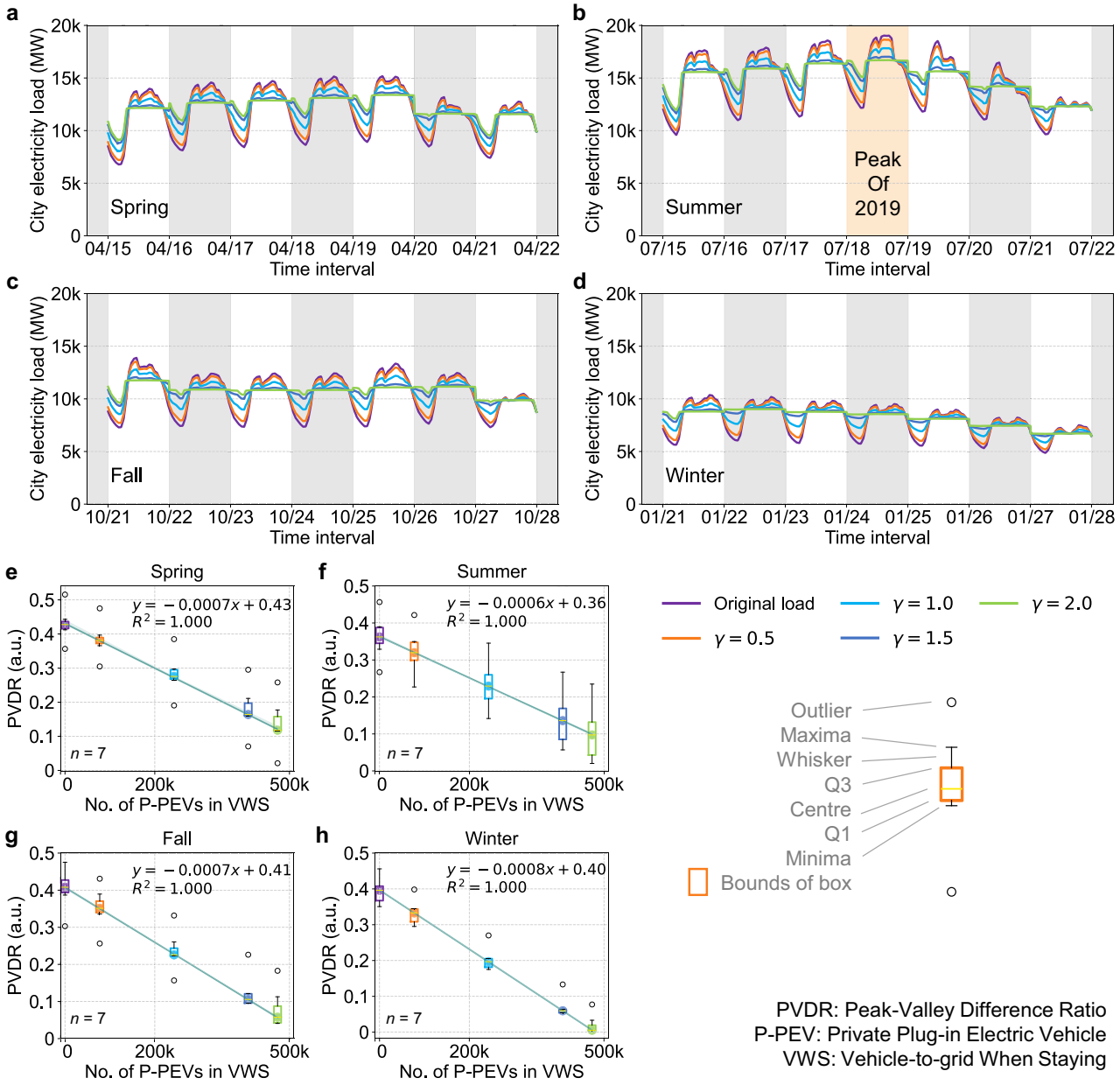

Fig. 6 | Illustration of Shenzhen load balancing performance of P-PEVs under different compensation rates. a–d The weekly curves of Shenzhen's original load and the load with V2G compensation ratio $\gamma = 0.5, 1.0, 1.5, 2.0$, respectively. The simulation is conducted in different overall load levels (spring, summer, fall, winter), where the annual peak occurs in summer. **e–h** The box plots which compare the daily peak-valley difference ratio (PVDR) of different load curves presented in Fig. 6a–d. Note that for each γ, the corresponding load curve is affected by both P-PEVs involved in VWS and ones in VWC, and the numeric relationship is shown in Fig. 7a. However, since the contributions of VWC are trivial (see Fig. 7b, c), we directly fit the relationship between PVDR and the number of P-PEVs involved in VWS in the boxplots.

except winter. This section investigates how V2G evaluation metrics evolve when enforcing minimum user satisfaction thresholds. Specifically, we denote user satisfaction after a V2G activity as ϵ^{usr}. We consider VWS, $\gamma = 2.0$ scenario with three thresholds $\epsilon^{usr} \geq 40\%, \epsilon^{usr} \geq 60\%, \epsilon^{usr} \geq 80\%$, respectively. Experiments are conducted for summer, spring and fall loads.

As shown in Fig. 8a, stricter satisfaction requirements differentially impact valley-filling performance across seasons. Notably, peak-shaving capability remains largely unaffected, except for two high-demand summer days when ϵ^{usr} is constrained to exceed 80%. In Fig. 8b, as ϵ^{usr} thresholds increase, the median PVDR values of three seasons are gradually lifted from 0.118, 0.098, 0.058 to 0.199, 0.184, 0.120, respectively. In Fig. 8c, the average weekly battery degradation costs across three seasons decline from 31.15, 29.41, 25.37 RMB (around 4.30–3.50 USD) to 17.47, 19.21, 17.20 RMB (around 2.41–2.37 USD), respectively. Similarly, the median values decrease from 31.82, 29.95, 26.30 RMB (around 4.39–3.63 USD) to 16.02, 17.94, 15.97 RMB (around 2.21–2.20 USD), respectively. In Fig. 8d, user satisfaction exhibits a significant improvement, with median values progressively increasing from 50.73%, 47.81%, 67.03% to 83.07%, 80.57%, 87.27%, respectively. In Fig. 8e, the total compensation costs for $\epsilon^{usr} \geq 40\%$ and $\epsilon^{usr} \geq 60\%$ exhibit both increases and decreases compared to the default scenario, whereas the total costs for $\epsilon^{usr} \geq 80\%$ consistently decrease relative to the baseline. Specifically, the reductions for $\epsilon^{usr} \geq 80\%$ reach 4.09 M, 1.43 M, and 2.24 M RMB (around 0.56M–0.31 M USD), respectively.

https://doi.org/10.1038/s41467-025-65073-8

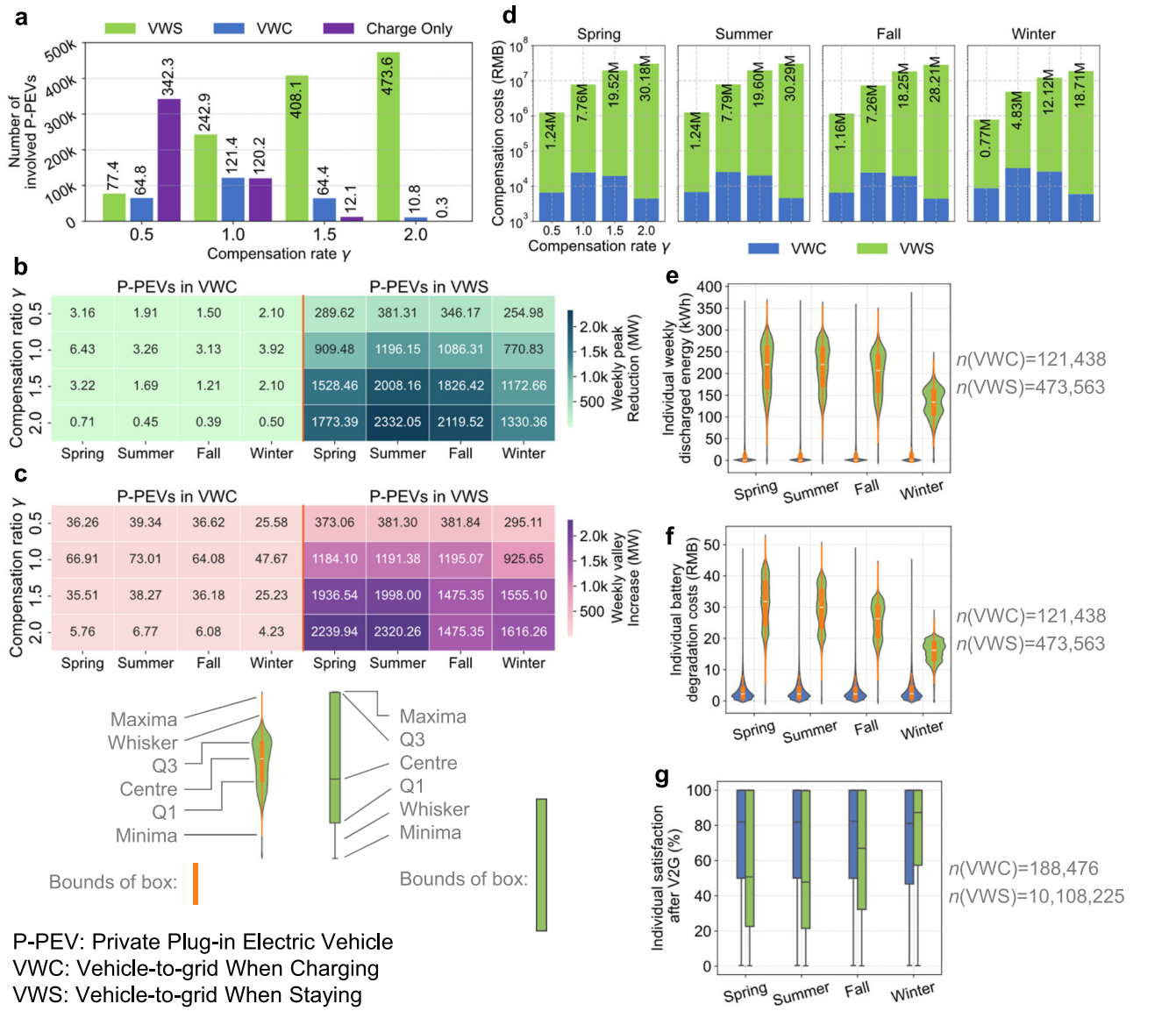

Fig. 7 | Evaluation of V2G effects under V2G When Charging (VWC) and V2G When Staying (VWS) with different compensation rates. a Numbers of P-PEVs participating in different V2G scenarios. **b**, **c** Contributions of VWC and VWS in reducing the city weekly peak load and increasing the city's weekly valley load, respectively. **d** Total compensation costs paid for users involved in VWC and VWS, respectively. **e** Distributions of individual weekly discharged energy under VWC and VWS. **f** Distributions of individual battery degradation costs under VWC and VWS. **g** Boxplots of individual satisfaction after a V2G activity.

To briefly summarize, maintaining high user satisfaction leads to a 30–40% reduction in battery degradation costs and a 5–13% decrease in total compensation costs, though with modest trade-offs in valley filling efficiency and limited peak shaving performance under extremely high-load conditions.

Extreme vehicle-to-grid imagination for China's megacities

MOVC has the transferability to other urban contexts. The generalization ability is utilized to explore two substantial problems: (1) How V2G effects evolve with larger P-PEV penetration rates, and (2) whether city-level upgrades in residential distribution grids for accommodating comprehensive QC are cost-effective. To this end, we illustrate the estimated P-PEV holdings of Beijing, Shanghai, Guangzhou and Shenzhen in 2024, reaching 640,000, 1,020,000, 650,000, and 760,000, respectively. The selected cities represent the most economically developed cities in China. We leverage 2022 BPTD to depict mobility and charging patterns of Beijing P-PEVs following the collective paradigm introduced in this study, as provided in Supplementary Figs. 2,4a,5, 13–16. We use 2022 BPTD to generate vehicles for Beijing's case, and use 2022 SPTD for Shanghai, Guangzhou and Shenzhen. We compare two V2G scenarios, namely (1) VWS (Default), where the settings are identical to the ones in Figs. 6 and 8, except for the number of involved P-PEVs. (2) VWS (QC 100%), where P-PEVs are allowed to use QC even in Home regions, and all the Park actions will perform VWS with QC power levels.

As shown in Fig. 9b–e, the discussed two scenarios exhibit similar load balancing effects with larger P-PEV penetration rates. Specifically, the weekly median PVDR values for all cities under VWS (Default) and VWS (QC 100%) are 0.0015, 0.0487, 0.0262, 0.0109 and 0.0015, 0.0015, 0.0016, 0.0092, respectively. Compared with PVDR of original loads (0.35, 0.41, 0.36, 0.36), extra benefits only reach 0%, 12%, 7%, 5%, respectively. In Fig. 9f–i, after full QC upgrades, the median values of weekly discharged energy in Beijing, Guangzhou and Shenzhen decrease from 151.25, 171.66, 147.04 kWh to 140.47, 154.21, 128.10 kWh, respectively. However, in Shanghai, where the overall city load is higher, the values increase from 237.30 to 252.20 kWh. Regarding

https://doi.org/10.1038/s41467-025-65073-8

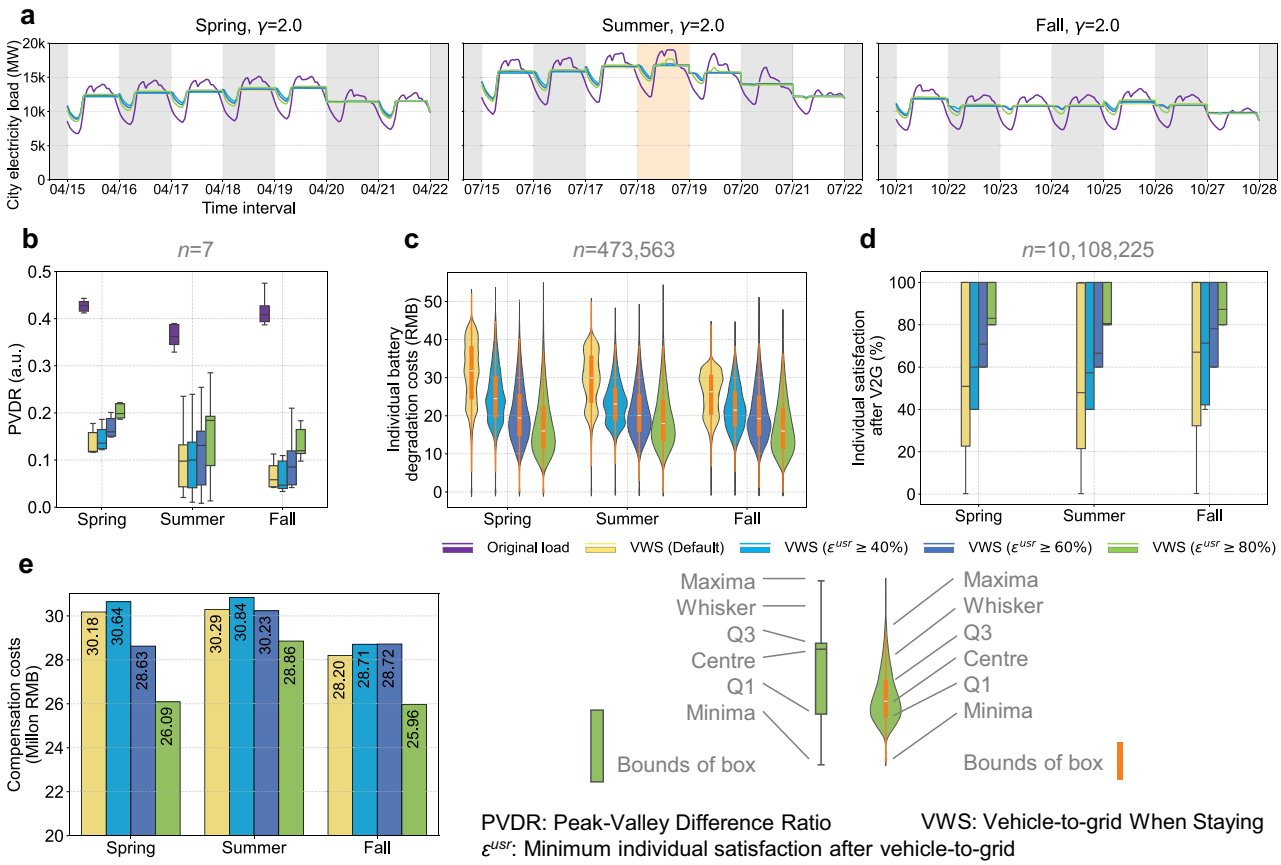

Fig. 8 | Evaluation of V2G effects under VWS, $\gamma = 2.0$ considering higher minimum satisfaction after V2G activities. a The weekly curves of Shenzhen's original load and the load under VWS, $\gamma = 2.0$, with minimum satisfaction $\epsilon^{usr} = 40\%, 60\%, 80\%$, respectively. The winter load is not considered since the median of the default VWS satisfaction in winter already exceeds 80% (see Fig. 7g). **b** PVDR with different minimum values of ϵ^{usr} in three seasons. **c** Distributions of individual battery degradation costs with different minimum values of ϵ^{usr} in three seasons. **d** Boxplots of user satisfaction after V2G activities. The whiskers of some boxplots merge with their quartile markers (Q1/Q3) due to particular data distribution features. **e** Total compensation costs paid with different minimum values of ϵ^{usr}.

battery degradation costs, the median values of Beijing, Guangzhou and Shenzhen decrease from 18.55, 28.54, 16.78 RMB (around 2.56-2.31 USD) to 17.54, 15.57, 13.19 RMB (around 2.42–1.82 USD), respectively. In contrast, the metric of Shanghai slightly increases from 29.87 to 30.71 RMB (around 4.12–4.24 USD). Another noteworthy effect is observed in Shenzhen's case. With the deeper P-PEV penetration, the median weekly discharged energy decreases from 220.29 kWh (Fig. 7e, summer) to 147.04–128.10 kWh, and the median battery costs also decrease from 29.95 RMB (around 4.13 USD, Fig. 7f, summer) to 16.78–13.19 RMB (around 2.31–1.82 USD). Notably, the inequity of both metrics in all cities grows significantly. For the weekly discharged energy, the standard deviation of all individuals increases from 46.05, 70.17, 39.00, 35.43 kWh to 60.85, 97.37, 65.74, 54.59 kWh, respectively. For the battery degradation costs, the metric goes up from 4.42, 6.82, 7.71, 3.83 RMB (around 0.61–0.53 USD) to 8.61, 12.61, 7.98, 6.30 RMB (around 1.19–0.87 USD).

The results indicate that as the number of V2G-related vehicles increases, cities with mild load profiles (Beijing, Guangzhou, Shenzhen) exhibit lighter optimization burdens to each vehicle, leading to lower discharged energy and battery degradation costs. In such cases, QC upgrades yield marginal additional benefits. Conversely, in cities with higher load levels (e.g., Shanghai), achieving comparable effects requires a higher penetration of P-PEVs. Additionally, expanding QC infrastructure significantly increases the variance of both discharged energy and degradation costs (Fig. 9f–i), enlarging the standard deviation by 32%–69% and 4%–95%, respectively. Customized V2G incentive policies may be required to mitigate such inequity. Given the substantial costs for residential grid upgrades, city policymakers should carefully weigh the trade-offs between investments and expected benefits.

Discussion

We present the MOVC framework to comprehensively describe the travel and energy usage patterns of P-PEVs. The framework manages to reconcile megacity-scale V2G scheduling with fine-grained consideration of heterogeneous driving and charging behaviors of users. Our findings answer how many battery storage resources remain underutilized among hundreds of thousands of P-PEVs in China's megacities, how effectively utilizing these resources can contribute to urban load shifting, and what the tradeoff is in terms of economic investment and user-centric factors. Additionally, we discuss the impacts of both higher P-PEV penetration rates and fully-covered QC under extreme assumptions.

An important feature of the MOVC framework is its decoupled perspective for megacity-scale V2G analysis. Owing to its modular architecture, the framework allows integration of diverse V2G studies with varying focus areas. For instance, the mobility model is interchangeable with other trip-chain models[71], graph-based OD models[34]. The charging behavior model is compatible with analysis on charging station data[76], large language model-based methods[77], or can incorporate user surveys[44,48,51] to support realistic city-specific studies. The V2G optimization can also be substituted with deep reinforcement learning paradigms[63–65]. However, some drawbacks exist in the proposed framework. First, the mobility model is not accurate enough in

https://doi.org/10.1038/s41467-025-65073-8

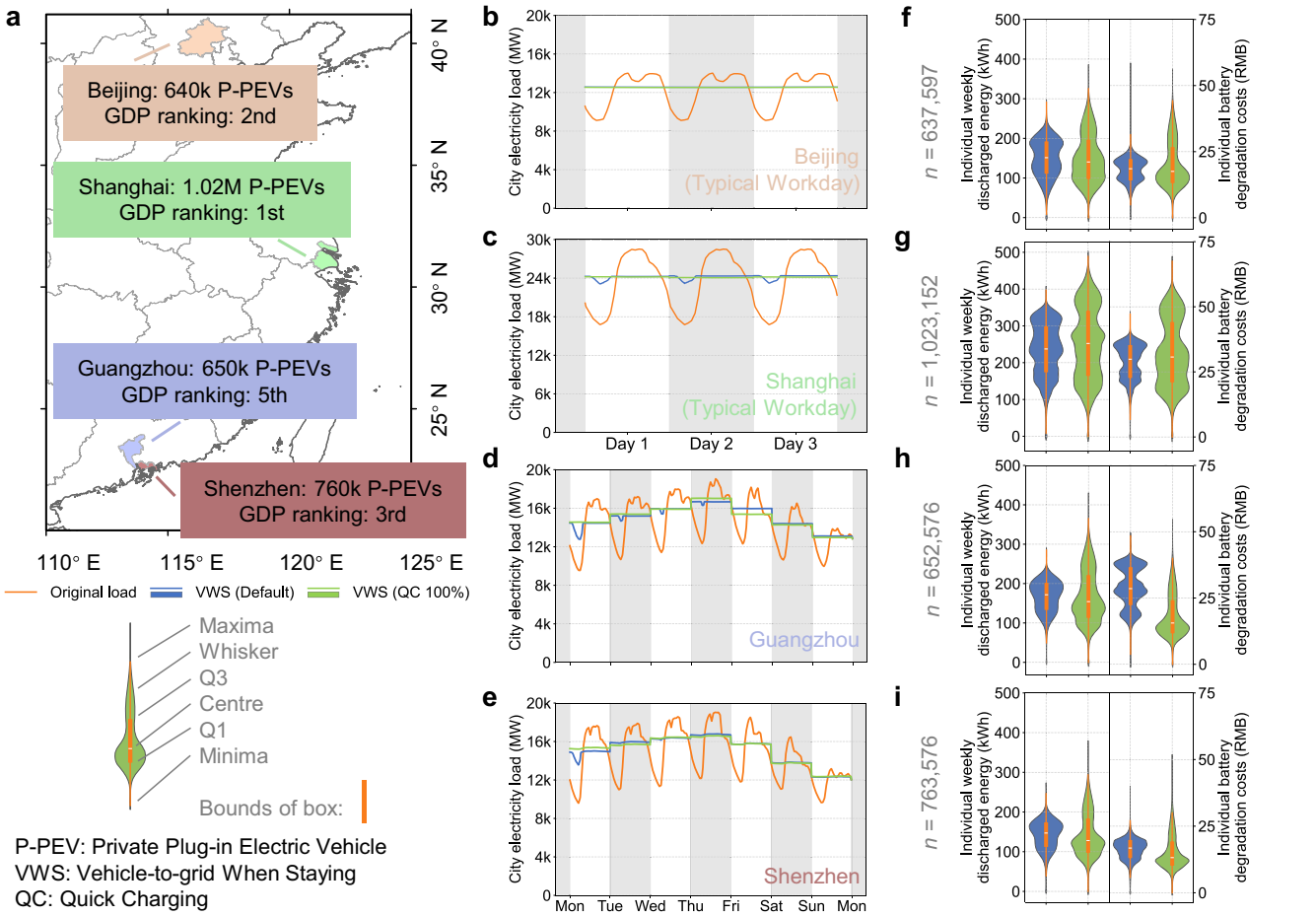

Fig. 9 | V2G evaluation in Beijing, Shanghai, Guangzhou and Shenzhen based on MOVC. a The partial map of China to show the P-PEV holdings of the four cities in 2024, and their GDP rankings in China's cities. **b**–**e** Load balancing results of the four cities under VWS (Default) and VWS (QC 100%), respectively. Since we do not have the annual load data of Beijing and Shanghai, we illustrate their results in typical workdays. For Guangzhou and Shenzhen, we select a week with the annual peak. **f**–**i** Distributions of individual weekly discharged energy and battery degradation costs under the two V2G scenarios.

predicting 0–2 km short distances, as shown in Fig. 3b. Second, the framework includes several economic metrics, but the primary objective is load shifting rather than a detailed cost-effectiveness analysis (e.g., Pareto fronts between load shifting effects and economic costs). Exploring the latter problem with proper relaxations or other efficiency techniques would support practical applications of V2G strategies. Third, the framework focuses on individual V2G scheduling and omits behavioral similarity that probably exists in a large number of P-PEVs. Given that P-PEVs will continue to proliferate rapidly in China, incorporating carefully designed clustering algorithms would further improve the computational efficiency.

In conclusion, the MOVC framework provides a feasible solution for megacity-scale V2G analysis, covering pre-scheduling factors (travel-charge behaviors, V2G participation) and post-scheduling ones (PVDR, compensation costs, battery degradation costs and user satisfaction). Results indicate that under Charge Only, P-PEV peak charging power only equals 2% of Shenzhen's peak load. Several variations of P-PEV charging patterns considering range anxiety, charging power, and charging costs are discussed, where the duration of Park actions consistently dominates. The observation motivates us to further discuss two V2G scenarios (VWC and VWS) and explore their combined effects under different compensation intensities. The weekly median PVDR of the original city load can be decreased up to 72.4–98.7% seasonally, where VWC and VWS-related vehicles release tens of MW and 2000 MW load balancing capacities, respectively, at compensation costs of 18.71M–30.29 M RMB (around 2.58M–4.18 M USD). However, lower costs can also attract a sufficient number of users to participate and yield decent load shifting outcomes. Furthermore, if considering higher user satisfaction after V2G activities, individual battery degradation costs and total compensation costs can be reduced by 30–40% and 5–13%, respectively, with an acceptable sacrifice on load balancing performance. A generalization study across China's megacities indicates that the imaginary residential QC upgrades offer marginal benefits in load balancing (0–12%) and battery lifespan, but may exacerbate individual energy scheduling inequity by 4–95%.

In the future, our work could be combined with operator-centric methods to schedule V2G in regional integrated energy systems with enriched traveling details towards an operator-user integrated manner. Additionally, as renewable energy penetration increases in power systems, future studies may discuss the P-PEV potential of modifying the demand side load curve to accommodate stronger fluctuations in the generation side.

Methods

Ethical approval is not required for this study, as it is based on fully anonymized data and does not involve human participants or personal information.

Datasets

In this study, we use a large volume of location data recorded by Bluetooth devices within P-PEVs, named the 2022 Shenzhen P-PEV

Trajectories Dataset and 2022 Beijing P-PEV Trajectories Dataset, provided by the Shenzhen Municipal Transport Bureau. The two datasets collect 9,108,081 and 9,651,948 location records from 36,932 and 38,129 P-PEV users primarily active in Shenzhen and Beijing, respectively, covering the dates between October 1, 2022, and December 31, 2022. Each record contains the anonymous user ID, timestamp, duration, latitude and longitude information. The data is used to extract stay/movement information and to generate user-specific behavior parameters to activate the Timegeo[28]-based mobility model.

We use the 2019 Shenzhen Parking Census Dataset provided by the Shenzhen Municipal Development and Reform Commission to visualize the distribution of depots. The dataset contains 9748 parking lots with information on their longitude, latitude, and the number of depots within.

We utilize the 2019 National PEV Big Data Statistics[78], which provides information on the daily average travel distance, monthly average charging times, QC charging and slow charging ratios, charging duration distribution of PEVs and other relevant information. We make use of this dataset to verify and calibrate our model.

We leverage the 2019 Shenzhen electricity load profile and the 2019 Guangzhou electricity load profile to obtain the city's original overall load. The data contains hourly load values for Shenzhen and Guangzhou over the entire year. We select a week's values of load data and interpolate them to match the 10-min interval resolution of the MOVC framework. For load profiles of Beijing and Shanghai, only typical workday load data is available. We thus replicate the single workday load pattern across several days for the following optimization. Data of load profiles is provided by China Southern Power Grid.

Private plug-in electric vehicle trajectories extraction

We define a stay as an activity at a specific location lasting over 10 min and within 300 square meters. Each square is defined as a cell to discretize the city map. Considering data accuracy and vehicle traveling characteristics, we merge all the extracted stay points into a stay region by applying a grid-based clustering algorithm (see Supplementary Fig. 1 and Note. 1). We label each cell in descending order based on the number of stay points they contain. Then, we merge the unlabeled cells with the labeled ones, resulting in a set of stay regions with a maximum range of 900 meters. Eventually, we divide Shenzhen's 1997.47 km^2 area into 3080 valid stay regions. Similarly, Beijing's 16410.54 km^2 area is decomposed into 18,118 valid stay regions.

After the above procedure, we obtain users' sequential action chains varying by time. We further categorize the stay regions as home, work, or other based on visit times and frequencies. Specifically, a visit that starts between 6 PM and 4 AM and ends before 12 AM will be labeled as a potential home-type visit. A Home label will be identified from a user's historical traveling records with the most home-type visits. When labeling workplaces, we assume that a longer trip has a higher probability for work purposes than a shorter one (e.g., shopping nearby). We thus leverage a utility function $U(d_i, n_i) = n_i \times d_i$ to describe the likelihood that a stay region will be marked as work-type for a user i, where n_i denotes the visit frequency and d_i denotes the distance from user i's home. As a result, we identify 22,779 users with work labels among 32,186 users with home labels. For Beijing, the numbers are 26,392 and 34,924, respectively. Details of determining Home and Work labels are given in Supplementary Note. 1.

Private plug-in electric vehicle mobility modeling

At the mobility level in our system, we modify the original TimeGeo[28] framework for P-PEV-oriented mobility modeling, using the extracted P-PEV trajectory information. In this framework, the continuous time is discretized into 10-min time slots, and in each time slot t, a temporal and spatial decision is made.

For temporal decisions, by introducing three PEV-specific parameters: a weekly home-based tour number (n_w), a dwell rate (β_1), and a burst rate (β_2), TimeGeo[28] builds a Markov chain model to calculate the probability to move or stay in each time slot, based on individual parameters and P(t). P(t) is defined as the weekly average travel circadian rhythm of the entire P-PEV population, for commuters and non-commuters separately (as shown in Supplementary Fig. 4b). Details of determining n_w, β_1 and β_2 are provided in Supplementary Note. 1 and Supplementary Figs. 2, 3. The specific probability of each choice is shown in Fig. 2.

For the P-PEV spatial decision, we modify the rank-based exploration and preferential return (r-EPR) mechanism to the gamma-distributed gravity-based EPR model. r-EPR first decides whether to explore a new place or to return to a previously visited one. The probability of the former choice is described as a function of visited location number S and personal tendency parameters ρ and γ:

$$P_{new} = \rho S^{-\gamma} \tag{1}$$

If the decision is to explore, the probabilities of visiting different locations should be specified. We denote the current location as SR^{ori} and the next potential location as SR^{des}. We couple the gravity model[79] and the gamma distribution to describe the probability of visiting SR^{des}, following

$$P(SR^{des}|SR^{ori}, d) = \frac{\rho(SR^{des})}{\mathrm{gamma(d)}} \tag{2}$$

where $\rho(SR^{des})$ refers to the visiting popularity index of the stay region SR^{des}, $\mathrm{gamma(d)} = \frac{\beta^\alpha}{\Gamma(\alpha)} d^{\alpha-1} e^{-\beta d}$ is a gamma distribution, and $d = |SR^{des} - SR^{ori}|$ denotes the distance between SR^{des} and SR^{ori}. α, β are the shape parameter and the rate parameter fitted from the trajectory datasets.

We separate PEVs into several S groups, and different groups possess different spatial exploration and preference parameters $\alpha, \beta, \rho, \gamma$, as shown in Supplementary Figs. 5 and 6.

To match the simulation scale with the number of P-PEVs in Shenzhen and Beijing, we expand the P-PEV number based on the parking spot densities across different districts of the city (see Supplementary Note. 1 and Supplementary Table. 4). Note that what we expand is the individual parameter set ($n_w, \beta_1, \beta_2, \alpha, \beta, \rho, \gamma$). Given two identical parameter sets, the simulated trajectories are not identical according to the above probabilistic conditions. We randomly allocate the P-PEV model to each user according to the market share information provided in Supplementary Table. 6.

User charging behavior modeling

We modify the utility-based charging behavior method[39] to establish our charging decision model. Available charging modes upon Stay arrivals are defined as $C_{i,s} = \{\mathrm{cm} : L_{\mathrm{cm}}^{i,s} = 1\}$ for the sth Stay of the ith P-PEV. We use $\mathrm{cm} = 0, 1, 2$ to refer to no-charging, slow charging and QC, respectively. Denote $V_{L_{\mathrm{cm}}^{i,s}}$ as the indirect utility of charging mode $L_{\mathrm{cm}}^{i,s}$. The choice probability of each charging mode is expressed as follows[39]:

$$P_{\mathrm{choice}_{i,s}}(L_{\mathrm{cm}}^{i,s}) = \begin{cases} \frac{\exp(V_{L_{\mathrm{cm}}^{i,s}})}{\sum_{j \in C_{i,s}} \exp(V_{L_{\mathrm{cm}}^{i,s}})} & \text{if } cm \in C_{i,s}, \\ 0 & \text{if } cm \notin C_{i,s}. \end{cases} \tag{3}$$

For the no-charging (Park) choice, we normalize the indirect utility to 0. Except for the extreme V2G case, we assume that slow charging is always available in all kinds of stay regions (Home, Work, Other), and QC is only available in public locations (Work, Other).

Furthermore, the indirect utility of the charging mode $L_{cm}^{i,s}$ is defined as

$$V_{L_{\mathrm{cm}}^{i,s}} = \beta_0 + V_{\mathrm{SOC}_{i,s}^e} + V_{R_{L_{\mathrm{cm}}^{i,s}}} + V_{\Delta\mathrm{SOC}_{L_{\mathrm{cm}}^{i,s}}} + V_{\mathrm{Cost}_{L_{\mathrm{cm}}^{i,s}}} + V_{\mathrm{Stay},\mathrm{L}_{\mathrm{cm}}^{\mathrm{i,s}}}, \mathrm{cm} \in \mathrm{C_{i,s}} \setminus \{0\}, \tag{4}$$

where β_0 is a constant representing the average effect of the non-listed attributes[39] set as 1 in the base case. Each component V_X refers to the utility of attribute X.

The first component $V_{\mathrm{SOC}_{i,s}^e}$ describes the relationship between the current SOC and user i's corresponding willingness to charge[39], which is modeled as

$$V_{\mathrm{SOC}_{i,s}^e} = \begin{cases} +\infty & \text{if } \mathrm{SOC}_{i,s}^e \in (0, \mathrm{SOC}_{i,s}^{\mathrm{dem}}] \\ \beta_{\mathrm{SOC}} \cdot \ln\left(\frac{1-\mathrm{SOC}_{i,s}^e}{(\frac{1}{\mathrm{SOC}_B}-1)\mathrm{SOC}_{i,s}^e}\right) & \text{if } \mathrm{SOC}_{i,s}^e \in (\mathrm{SOC}_{i,s}^{\mathrm{dem}}, 1) \\ -\infty & \text{if } \mathrm{SOC}_{i,s}^e = 1 \end{cases} \tag{5}$$

Where SOC_B is the range buffer set as 0.3, $\mathrm{SOC}_{i,s}^e$ is the current SOC, β_{SOC} is set as 3 in the base case, and $\mathrm{SOC}_{i,s}^{\mathrm{dem}}$ refers to the moving consumption of the sequential three trips.

The second component $V_{R_{L_{\mathrm{cm}}^{i,s}}}$ describes user i's preference toward high charging power[39], defined as

$$V_{R_{L_{\mathrm{cm}}^{i,s}}} = \beta_R \cdot (P_{L_{\mathrm{cm}}^{i,s}} - P_{\mathrm{home}}), \tag{6}$$

where $P_{L_{\mathrm{cm}}^{i,s}}$ is the charging power of charging mode $L_{\mathrm{cm}}^{i,s}$, P_{home} is the charging power at Home, and β_R is a coefficient. A larger β_R indicates that the user prefers faster charging to reduce the charging duration, and a smaller one shows their tendency to avoid battery degradation. In our base case, β_R is set as 0.

The third component $V_{\Delta\mathrm{SOC}_{L_{\mathrm{cm}}^{i,s}}}$ refers to user i's evaluation of the potential energy he can obtain during Stay s. Generally, the utility of this attribute is designed to increase when a larger amount of energy can be expected to charge during Stay s[39]. The formulation is

$$V_{\Delta\mathrm{SOC}_{L_{\mathrm{cm}}^{i,s}}} = \beta_{\Delta\mathrm{SOC}} \cdot [1 - (\Delta\mathrm{SOC}_{L_{\mathrm{cm}}^{i,s}} - 1)^2], \tag{7}$$

where $\Delta\mathrm{SOC}_{L_{\mathrm{cm}}^{i,s}} = \min\left(\frac{P_{L_{\mathrm{cm}}} \cdot T_{i,s}}{E_i}, 1 - \mathrm{SOC}_{i,s}^e\right)$ represents the potential increased energy under charging mode $L_{\mathrm{cm}}^{i,s}$, $P_{L_{\mathrm{cm}}}$ is the corresponding charging power, $T_{i,s}$ is the duration of Stay s, E_i is the battery capacity, and $\mathrm{SOC}_{i,s}^e$ is the SOC of P-PEV i upon arrival of Stay s. $\beta_{\Delta\mathrm{SOC}}$ is the coefficient set as 3 in the base case.

The fourth component $V_{\mathrm{Cost}_{L_{\mathrm{cm}}^{i,s}}}$ describes users' sensitiveness of charging costs. Differing from the constant electricity price setting[39], we introduce a ToU price to represent a more realistic cost evaluation. Specifically, the charging cost $\mathrm{Cost}_{L_{\mathrm{cm}}^{i,s}}$ is designed as

$$\mathrm{Cost}_{L_{\mathrm{cm}}^{i,s}} = \sum_{t=Ta_{i,s}}^{Td_{i,s}} P_{L_{\mathrm{cm}}^{i,s},t}^{\mathrm{ToU}} \cdot \mathrm{SOC}_{L_{\mathrm{cm}}^{i,s},t} \cdot E_i, \tag{8}$$

where $Ta_{i,s}$, $Td_{i,s}$ refer to the arrival and departure time slots of user i, Stay s, respectively. $P_{L_{\mathrm{cm}},t}^{\mathrm{ToU}}$ denotes the ToU price at time slot t. The utility $V_{\mathrm{Cost}_{L_{\mathrm{cm}}^{i,s}}}$ is computed following

$$V_{\mathrm{Cost}_{L_{\mathrm{cm}}^{i,s}}} = -\beta_{\mathrm{Cost}} \cdot (\mathrm{Cost}_{L_{\mathrm{cm}}^{i,s}} - \mathrm{Cost}_{\mathrm{home}}), \tag{9}$$

where β_{Cost} is set as 0.35 in the base case, and $\mathrm{Cost}_{\mathrm{home}}$ can also be calculated following Eq. (8). The only distinction is that $\mathrm{Cost}_{L_{\mathrm{cm}}^{i,s}}$ uses $P_{L_{\mathrm{cm}},t}^{\mathrm{ToU,pub}}$ and $\mathrm{Cost}_{\mathrm{home}}$ uses $P_{L_{\mathrm{cm}},t}^{\mathrm{ToU,home}}$, representing different ToU price of public and private charging piles, respectively, and the former is generally more expensive. The details of ToU price are obtained from charging service providers[75] and are given in Supplementary Fig. 7.

The last component $V_{\mathrm{Stay},\mathrm{L}_{\mathrm{cm}}^{\mathrm{i,s}}}$ is added to simulate users' patterns of slow charging decisions. We assume that either a too-short or a too-long stay duration will decrease the users' willingness to perform slow charging. $V_{\mathrm{Stay},\mathrm{L}_{\mathrm{cm}}^{\mathrm{i,s}}}$ is thus given as

$$V_{\mathrm{Stay},L_{\mathrm{cm}}^{i,s}} = \begin{cases} \max(\beta_{\mathrm{Stay}} \cdot (T_{i,s} - 2) \cdot (T_{i,s} - 10), B_{\mathrm{Stay}}) & \text{if cm} = 1 \\ 0 & \text{if cm} \in \{0, 2\} \end{cases} \tag{10}$$

where the coefficient β_{Stay} and the buffer B_{Stay} are set as −0.2 and −3, respectively.

We provide settings of $\beta_0, \beta_{\mathrm{SOC}}, \beta_R, \beta_{\mathrm{SOC}}, \beta_{\mathrm{Cost}}$ and β_{Stay} under different charging cases in Supplementary Table. 5.

We model the energy consumption during traveling using the drivetrain losses[74], defined as:

$$P_{dr} = \alpha V^3 + \beta V^2 + \gamma V + P_{stop}, \tag{11}$$

where V denotes the average velocity of the trip, and we set $\alpha = 9.494 * 10^{-6}$, $\beta = 1.93 * 10^{-4}$, $\gamma = 0.0506$, $P_{stop} = 2.375$.

Coupling mobility and charging

The mobility model and the charging model are executed sequentially. We start with the mobility model, which provides us with the information of stay durations and locations. Afterwards, we freeze the results of the mobility model and generate user-intended charging behaviors following Eqs. (3)–(11). Finally, we fix the charging decisions of users and perform V2G-related optimization. The mobility patterns and the charging behaviors are simulated for 8 weeks, taking the first 2 weeks to reach a steady state. The initial values of V2G optimization are set as a specific time slot within the steady state. Related objectives and constraints are illustrated in the following section.

Vehicle-to-grid participation modeling

We modify the previous work[46] to simulate users' responses to different V2G strategies under various incentives. Specifically, we introduce customer damage cost (CDC) to reflect users' concerns about convenience and battery degradation. CDC can be regarded as the economic compensation required by P-PEV users for participating in V2G. Denote the average and standard deviation of CDC for P-PEV users as μ_c and δ_c. For P-PEV i, the CDC is ξ^i following the normal distribution:

$$\xi^i \text{obeys } N(\mu_c, \delta_c) \tag{12}$$

In practice, μ_c and δ_c are assumed to be known to the policy makers. They need to determine the unit V2G compensation rate γ, and the P-PEV users considering accepting V2G control fulfill Eq. (13)[46]:

$$\xi^i \le \gamma \cdot \mu_c \tag{13}$$

The economic costs f^{cc} to compensate CDC are calculated as follows:

$$f^{cc} = \gamma \cdot \mu_c \sum_{i=1}^{N} \sum_{t=1}^{T} P_{i,t}^{dis} \tag{14}$$

Since our research considers two V2G strategies, we set $\mu_c^{VWS} = 0.15$ RMB (around 0.02 USD) per kWh, $\delta_c^{VWS} = 0.075$ RMB (around 0.01 USD) per kWh to compensate users involved in V2G

When Staying, and set $\mu_c^{VWC} = 0.03$ RMB (around 0.004 USD) per kWh, $\delta_c^{VWC} = 0.015$ RMB (around 0.002 USD) per kWh for users involved in V2G When Charging. We set four levels of compensation rate γ as $\gamma = 0.5, 1, 1.5, 2$, respectively. We provide a more detailed flowchart of our V2G participation mechanism in Supplementary Fig. 9.

Modeling urban load optimization via vehicle-to-grid

The scale of the optimization problem we consider is immense, involving the allocation of charging and discharging behaviors for up to 1,020,000 electric vehicles over 1 week (1008 time intervals). To balance computational complexity and model accuracy, we propose an LP model.

Our LP model is formulated as follows:

$$\begin{aligned}&\min f_1 + \lambda \cdot f_2 \\ &= \frac{1}{T}\sum_{t=1}^{T} Dev_t + \lambda \cdot \frac{1}{T}\sum_{i=1}^{N}\sum_{t=1}^{T}\left(P_{i,t}^{ch} + P_{i,t}^{dis}\right)\end{aligned} \tag{15}$$

s.t.

for $i = 1,2,\ldots,N$:
for $t \in [t_i^{arr}, t_i^{dep}]$:
if $A_{i,t}$ = park:

$$P_{i,t}^{ch} = 0 \tag{16}$$

$$P_{i,t}^{dis} = 0 \tag{17}$$

$$E_{i,t+1} = E_{i,t} \tag{18}$$

if $A_{i,t}$ = charge:

$$E_{i,t}/E_i^{\max} \geq 0 \tag{19}$$

$$E_{i,t}/E_i^{\max} \leq 1 \tag{20}$$

$$0 \leq P_{i,t}^{ch} \leq C_i^{ch} \tag{21}$$

$$0 \leq P_{i,t}^{dis} \leq C_i^{ch} \tag{22}$$

$$E_{i,t+1} = E_{i,t} + \eta P_{i,t}^{ch}/6 - P_{i,t}^{dis}/6/\eta \tag{23}$$

$$E_{i,t_i^{dep}} \geq E_{i,t_i^{dep}}^{need} \tag{24}$$

if $A_{i,t}$ = QC:

$$E_{i,t}/E_i^{\max} \geq 0 \tag{25}$$

$$E_{i,t}/E_i^{\max} \leq 1 \tag{26}$$

$$0 \leq P_{i,t}^{ch} \leq C_i^{QC} \tag{27}$$

$$0 \leq P_{i,t}^{dis} \leq C_i^{QC} \tag{28}$$

$$E_{i,t+1} = E_{i,t} + \eta P_{i,t}^{ch}/6 - P_{i,t}^{dis}/6/\eta \tag{29}$$

$$E_{i,t_i^{dep}} \geq E_{i,t_i^{dep}}^{need} \tag{30}$$

for $t \notin [t_i^{arr}, t_i^{dep}]$:

$$E_{i,t+1} = E_{i,t} - L_{t_i^{dep}}^{Move}/T_{t_i^{dep}}^{Move} \tag{31}$$

$$P_{i,t}^{ch} = 0 \tag{32}$$

$$P_{i,t}^{dis} = 0 \tag{33}$$

We set the optimization duration T to 1008. We set up the constraints by considering all possible P-PEV activities (Park, Charge, QC and Move). The staying and moving states of EVs are straightforward to model as shown in Eqs. (16), (17), (32), (33) and Eqs. (18), (31). As for charging and QC, we use Eqs. (19), (20), (25), (26) to constrain the maximum/minimum SOC of EVs, and utilize Eqs. (21), (22), (27), (28) to constrain the charging and discharging power limits. Here, $E_i^{\max}$, C_i^{ch} and C_i^{QC} are constants, and we assume that the maximum values of charging and discharging power are identical. Equations (23), (29) describe the change in the EV's battery energy from time t to $t+1$, where η denotes the battery efficiency. In our experiments, we set $\eta = 0.9$.

Equations (24), (30) claim that the P-PEV's energy at the departure time must not be less than the user's required energy E_{need}, which is a necessary condition to ensure that the user's travel plans are not affected. We take the minimum value from the two candidates as the value of E_{need}. The former is the total energy consumption due to mobility over the next 24 h, and the latter is the same consumption until the next charging session.

Objective Eq. (15) is designed to balance solution accuracy and computational efficiency. The f_1 term is our primary optimization objective, where Dev_t is used for evaluating the deviation between the overall load variables L_d^{sum} and an optimizable variable L_d^{avg}. Dev_t is constrained as follows:

$$\text{Dev}_t \leq |L_t^{\text{sum}} - L_{t//144}^{\text{avg}}| \tag{34}$$

where L^{avg} is a set of optimizable variables divided by calendar days, representing the desired average load value within a given day. L_t^{sum} is obtained by summing the city's original load L_t^{gt} with the total charging and discharging power given by the optimization model at time t, as follows:

$$L_t^{\text{sum}} = L_t^{gt} + \sum_{i=1}^{N}(P_{i,t}^{ch} - P_{i,t}^{dis}). \tag{35}$$

We select 4 weeks from the 2019 Shenzhen electricity load profile in spring, summer, fall and winter, respectively. We avoid Chinese public holidays (e.g., Spring Festival) to ensure the representativeness. To avoid introducing non-linear constraints, we rewrite Eq. (34) as follows:

$$\text{Dev}_t \geq L_t^{\text{sum}} - L_{t//144}^{\text{avg}} \tag{36}$$

$$\text{Dev}_t \geq L_{t//144}^{\text{avg}} - L_t^{\text{sum}} \tag{37}$$

The second weighted term f_2 in Eq. (15) is used to avoid simultaneous charging and discharging (SCD)[59–61]. Typically, when optimizing V2G behavior, complementarity constraints e.g., 0–1 variables or non-linear constraints $P_{i,t}^{ch} * P_{i,t}^{dis} = 0$ are used to prevent the EV from having non-zero charging and discharging power at a given time t. However, introducing a large number of 0–1 variables or using non-linear constraints will significantly increase the computation time to an unacceptable level. Therefore, we introduce f_2 to eliminate SCD. We

provide numerical results in Supplementary Fig. 11 to show the significant difference in computation time between our solution and the one with 0–1 variables, and we illustrate different designs of f_2 and the respective weights to avoid SCD in Supplementary Fig. 12. We solve the optimization using the Gurobi solver, setting the value of λ to 0.15. In practice, we optimize $N = 3000$ P-PEVs in a batch due to the capacity limitation of our platform. The results indicate that, without complementary constraints, optimizing N EVs over T intervals with $f_1 + \lambda \cdot f_2$ produces 0 records of SCD, compared to about 20% when optimizing with f_1 only. Supplementary Table. 7 shows the difference of constraints used in optimizing V2G When Charging and V2G When Staying.

Computation of charging potential and discharging potential

Charging potential $CP_{i,s}$ is the maximum capacity of a P-PEV i to absorb electricity in a Stay s. $CP_{i,s}$ is computed following

$$CP_{i,s} = \min(100, \mathrm{SOC}^{e}_{i,s} + P_i{*}T_{i,s}), \tag{38}$$

where $\mathrm{SOC}^{e}_{i,s}$ denotes the arrival SOC of Stay s, P_i denotes the slow charging power of P-PEV i, and $T_{i,s}$ refers to the duration of Stay s. Similarly, discharging potential $DP_{i,s}$ is defined as follows:

$$\mathrm{DP}_{i,s} = \max(\mathrm{SOC}^{\mathrm{need}}_{i,s}, \mathrm{SOC}^{e}_{i,s} - P_i{*}T_{i,s}), \tag{39}$$

where $\mathrm{SOC}^{\mathrm{need}}_{i,s}$ is the SOC format of E^{need} as introduced above. Capacity limit and SOC demand are set as 100 and $\mathrm{SOC}^{\mathrm{need}}_{i,s}$, respectively. Since we only consider Stay vehicles in time slot t, the values of both limits will vary with time.

User satisfaction after vehicle-to-grid activities

We evaluate user satisfaction after each V2G activity through Eq. (40)[67]:

$$\epsilon^{usr}_{i,s} = \frac{\mathrm{SOC}_{k,i,s}}{\mathrm{SOC}^{*}_{k,i,s}}{*}100\%, \tag{40}$$

where $\mathrm{SOC}_{k,i,s}$ denotes the actual SOC level after a V2G activity in Stay s, and $\mathrm{SOC}^{*}_{k,i,s}$ denotes the desired SOC level of the user i upon departure, which can be calculated following Eqs. (3), (11). $\epsilon^{usr}_{i,s}$ with values larger than 100% are set as 100%.

Equation (40) is regarded as an evaluation metric after V2G optimization. For scenarios with inferior satisfaction (e.g., spring, summer, fall), we illustrate optimization results with a stricter constraint to the SOC level upon departure in Fig. 8. The constraints are added as follows:

$$E_{i,t_i^{\mathrm{dep}}} \geq E^{*}_{i,t_i^{\mathrm{dep}}} \cdot \epsilon^{usr,th}, \tag{41}$$

where $E^{*}_{i,t_i^{dep}}$ is the desired energy level of user i upon departure time t_i^{dep}, and $\epsilon^{usr,th}$ denotes a minimum satisfaction threshold that must be reached at t_i^{dep}. We set $\epsilon^{usr,th}$ as 40, 60, and 80% in our experiments.

Battery degradation modeling

General quantification of battery degradation requires information on operating temperature, operating current, internal resistance, and calendar aging effects, which can hardly be obtained for large-scale P-PEVs. Therefore, we focus on cycling aging costs based on previous works[56,80,81]. The depth of discharge (DoD) of P-PEV i is denoted as $D_{i,t} = 1 - \frac{E_{i,t}}{E_i^{\max}}$, where $E_{i,t}$ can be determined following either Eqs. (3), (11) or V2G formulations in Eqs. (15), (33), and $E_i^{\max}$ is the maximum battery capacity of P-PEV i. Then the DoD-number of cycles (NC) curve can be fitted via measurement[56]:

$$\phi(D_{i,t}) = k_1 D_{i,t}^{k_2} + k_3, \tag{42}$$

where k_1, k_2, k_3 are coefficients describing the relationship between NC and DoD. We set $k_1 = 1.4{*}10^5, k_2 = -5.01{*}10^{-1}, k_3 = -1.23{*}10^5$, respectively[56]. The degradation costs of P-PEV i in time slot t with respect to DoD can be calculated as follows[56,80,81]:

$$C^{D}_{i,t} = |\frac{1}{\phi(D_{i,t})} - \frac{1}{\phi(D_{i,t-1})}| B_i^{\mathrm{cost}}, \tag{43}$$

where $\phi(D_{i,t})$ and $\phi(D_{i,t-1})$ are the NC at $\mathrm{DoD} = D_{i,t}$ and $D_{i,t-1}$, respectively. The battery investment cost B_i^{cost} is given as:

$$B_i^{\mathrm{cost}} = b_i^{\mathrm{cost}} \cdot E_i^{\max}, \tag{44}$$

where b_i^{cost} is the coefficient set as 957 RMB (132 USD) per kWh[56].

Reporting summary

Further information on research design is available in the Nature Portfolio Reporting Summary linked to this article.

Data availability

The data generated in this study have been partially deposited at the CodeOcean repository here[82]. Full data are available under restricted access for related confidentiality agreements, access can be obtained by contacting the corresponding author. Source data for reproducing the figures are available at Figshare repository here[83]. Source data are provided as a Source Data file. Source data are provided with this paper.

Code availability

The Python scripts developed for data analysis have been deposited at the CodeOcean repository here[82].

References

1. Xi, J. *Xi Jinping Delivers an Important Speech at the General Debate of the 75th Session of the United Nations (UN) General Assembly*, <http://ch.china-embassy.gov.cn/ger/zgxw/202009/t20200924_3208100.html> (UN, 2020).
2. Shao, T. et al. China's industrial decarbonization in the context of carbon neutrality: a sub-sectoral analysis based on integrated modelling. *Renew. Sustain. Energy Rev.* **170**, 112992 (2022).
3. Energy Transitions Commission *China 2050: A Fully Developed Rich Zero-Carbon Economy* (Energy Transitions Commission, 2019).
4. Silva, B. N., Khan, M. & Han, K. Futuristic sustainable energy management in smart environments: a review of peak load shaving and demand response strategies, challenges, and opportunities. *Sustainability* **12**, 5561 (2020).
5. Tao, S. et al. Non-destructive degradation pattern decoupling for early battery trajectory prediction via physics-informed learning. *Energy Environ. Sci.* **18**, 1544–1559 (2025).
6. Tao, S. et al. Generative learning assisted state-of-health estimation for sustainable battery recycling with random retirement conditions. *Nat. Commun.* **15**, 10154 (2024).
7. Tao, S. et al. Rapid and sustainable battery health diagnosis for recycling pretreatment using fast pulse test and random forest machine learning. *J. Power Sources* **597**, 234156 (2024).
8. Tao, S. et al. Collaborative and privacy-preserving retired battery sorting for profitable direct recycling via federated machine learning. *Nat. Commun.* **14**, 8032 (2023).
9. Tao, S. et al. Battery cross-operation-condition lifetime prediction via interpretable feature engineering assisted adaptive machine learning. *ACS Energy Lett.* **8**, 3269–3279 (2023).

10. Tao, S. et al. Immediate remaining capacity estimation of heterogeneous second-life lithium-ion batteries via deep generative transfer learning. *Energy Environ. Sci.* **18**, 7413–7426 (2025).
11. Gnann, T., Klingler, A.-L. & Kühnbach, M. The load shift potential of plug-in electric vehicles with different amounts of charging infrastructure. *J. Power Sources* **390**, 20–29 (2018).
12. López, M. A., De La Torre, S., Martín, S. & Aguado, J. A. Demand-side management in smart grid operation considering electric vehicles load shifting and vehicle-to-grid support. *Int. J. Electr. Power Energy Syst.* **64**, 689–698 (2015).
13. Kinhekar, N., Padhy, N. P. & Gupta, H. O. Multiobjective demand side management solutions for utilities with peak demand deficit. *Int. J. Electr. Power Energy Syst.* **55**, 612–619 (2014).
14. Cao, S. The impact of electric vehicles and mobile boundary expansions on the realization of zero-emission office buildings. *Appl. Energy* **251**, 113347 (2019).
15. Barone, G., Buonomano, A., Forzano, C., Giuzio, G. F. & Palombo, A. Increasing self-consumption of renewable energy through the building to vehicle to building approach applied to multiple users connected in a virtual micro-grid. *Renew. Energy* **159**, 1165–1176 (2020).
16. Tang, X. et al. Naturalistic data-driven predictive energy management for plug-in hybrid electric vehicles. *IEEE Trans. Transp. Electrif.* **7**, 497–508 (2020).
17. Ioakimidis, C. S., Thomas, D., Rycerski, P. & Genikomsakis, K. N. Peak shaving and valley filling of power consumption profile in non-residential buildings using an electric vehicle parking lot. *Energy* **148**, 148–158 (2018).
18. Wolinetz, M., Axsen, J., Peters, J. & Crawford, C. Simulating the value of electric-vehicle–grid integration using a behaviourally realistic model. *Nat. Energy* **3**, 132–139 (2018).
19. Xiong, Z., Shen, X., Wu, Q., Guo, Q. & Sun, H. Stochastic planning for low-carbon building integrated energy system considering electric-heat-V2G coupling. *Int. J. Electr. Power Energy Syst.* **151**, 109148 (2023).
20. Zhang, Y., Han, X., Wei, T., Zhao, X. & Zhang, Y. Techno-environmental-economical performance of allocating multiple energy storage resources for multi-scale and multi-type urban forms towards low carbon district. *Sustain. Cities Soc.* **99**, 104974 (2023).
21. Buonomano, A. Building to vehicle to building concept: a comprehensive parametric and sensitivity analysis for decision making aims. *Appl. Energy* **261**, 114077 (2020).
22. Liu, B. et al. Regional differences in China's electric vehicle sales forecasting: Under supply-demand policy scenarios. *Energy Policy* **177**, 113554 (2023).
23. Li, X., Peng, Y., He, Q., He, H. & Xue, S. Development of new-energy vehicles under the carbon peaking and carbon neutrality strategy in China. *Sustainability* **15**, 7725 (2023).
24. National Development and Reform Commission *Implementation Opinions on Strengthening the Integration and Interaction of New Energy Vehicles and Power Grids (in Chinese)*, https://www.ndrc.gov.cn/xxgk/zcfb/tz/202401/t20240104_1363096.html (National Development and Reform Commission, 2023).
25. Hu, J. et al. Vehicle travel destination prediction method based on multi-source data. *Automot. Innov.* **4**, 315–327 (2021).
26. Yuan, K., Song, Y., Shao, Y., Sun, C. & Wu, Z. A charging strategy with the price stimulus considering the queue of charging station and EV fast charging demand. *Energy Procedia* **145**, 400–405 (2018).
27. Yi, Z., Liu, X. C. & Wei, R. Electric vehicle demand estimation and charging station allocation using urban informatics. *Transp. Res. Part D Transp. Environ.* **106**, 103264 (2022).
28. Jiang, S. et al. The TimeGeo modeling framework for urban mobility without travel surveys. *Proc. Natl. Acad. Sci.* **113**, E5370–E5378 (2016).
29. Wang, Y. & Infield, D. Markov Chain Monte Carlo simulation of electric vehicle use for network integration studies. *Int. J. Electr. Power Energy Syst.* **99**, 85–94 (2018).
30. Yi, Z. et al. An agent-based modeling approach for public charging demand estimation and charging station location optimization at urban scale. *Comput. Env. Urban Syst.* **101**, 101949 (2023).
31. Yan, J. et al. EV charging load simulation and forecasting considering traffic jam and weather to support the integration of renewables and EVs. *Renew. energy* **159**, 623–641 (2020).
32. Wu, S. & Pang, A. Optimal scheduling strategy for orderly charging and discharging of electric vehicles based on spatio-temporal characteristics. *J. Clean. Prod.* **392**, 136318 (2023).
33. Xiang, Y. et al. Electric vehicle charging in smart grid: A spatial-temporal simulation method. *Energy* **189**, 116221 (2019).
34. Zhao, Y., Cheng, S., Gao, S., Wang, P. & Lu, F. Predicting origin-destination flows by considering heterogeneous mobility patterns. *Sustain. Cities Soc.* **118**, 106015 (2025).
35. Yi, Z. et al. A highly efficient control framework for centralized residential charging coordination of large electric vehicle populations. *Int. J. Electr. Power Energy Syst.* **117**, 105661 (2020).
36. Jian, L., Zheng, Y. & Shao, Z. High efficient valley-filling strategy for centralized coordinated charging of large-scale electric vehicles. *Appl. Energy* **186**, 46–55 (2017).
37. Zheng, Y., Shao, Z., Zhang, Y. & Jian, L. A systematic methodology for mid-and-long term electric vehicle charging load forecasting: the case study of Shenzhen, China. *Sustain. Cities Soc.* **56**, 102084 (2020).
38. Wang, Y., Yao, E. & Pan, L. Electric vehicle drivers' charging behavior analysis considering heterogeneity and satisfaction. *J. Clean. Prod.* **286**, 124982 (2021).
39. Liu, Y. S., Tayarani, M. & Gao, H. O. An activity-based travel and charging behavior model for simulating battery electric vehicle charging demand. *Energy* **258**, 124938 (2022).
40. Zheng, Y., Shao, Z. & Jian, L. The peak load shaving assessment of developing a user-oriented vehicle-to-grid scheme with multiple operation modes: the case study of Shenzhen, China. *Sustain. Cities Soc.* **67**, 102744 (2021).
41. Giordano, F., Diaz-Londono, C. & Gruosso, G. Comprehensive aggregator methodology for evs in v2g operations and electricity markets. *IEEE Open J. Veh. Technol.* **4**, 809–819 (2023).
42. Liang, H., Liu, Y., Li, F. & Shen, Y. Dynamic economic/emission dispatch including PEVs for peak shaving and valley filling. *IEEE Trans. Ind. Electron.* **66**, 2880–2890 (2018).
43. Zhou, K., Cheng, L., Lu, X. & Wen, L. Scheduling model of electric vehicles charging considering inconvenience and dynamic electricity prices. *Appl. Energy* **276**, 115455 (2020).
44. Ghotge, R., Nijssen, K. P., Annema, J. A. & Lukszo, Z. Use before you choose: What do EV drivers think about V2G after experiencing it?. *Energies* **15**, 4907 (2022).
45. Liu, K. & Liu, Y. Incentive-willingness-decision framework: Unit discharge triangle-based maximum stable V2G capability evaluation. *Appl. Energy* **374**, 123850 (2024).
46. Wang, X., Nie, Y. & Cheng, K.-W. E. Distribution system planning considering stochastic EV penetration and V2G behavior. *IEEE Trans. Intell. Transp. Syst.* **21**, 149–158 (2019).
47. Zhao, A. P., Li, S., Alhazmi, M., Bao, Z. & Cheng, X. Psychological insights and robust optimization in V2g: towards sustainable energy participation. *Int. J. Electr. Power Energy Syst.* **171**, 110931.
48. Geske, J. & Schumann, D. Willing to participate in vehicle-to-grid (V2G)? Why not!. *Energy Policy* **120**, 392–401 (2018).
49. Al-obaidi, A. A. & Farag, H. E. Optimal design of V2G incentives and V2G-capable electric vehicles parking lots considering cost-benefit financial analysis and user participation. *IEEE Trans. Sustain. Energy* **15**, 454–465 (2023).

50. Gupta, V., Kumar, R. & Panigrahi, B. K. User-willingness-based decentralized EV charging management in multiaggregator scheduling. *IEEE Trans. Ind. Appl.* **56**, 5704–5715 (2020).
51. van Heuveln, K. et al. Factors influencing consumer acceptance of vehicle-to-grid by electric vehicle drivers in the Netherlands. *Travel Behav. Soc.* **24**, 34–45 (2021).
52. Singh, K. & Singh, A. Behavioural modelling for personal and societal benefits of V2G/V2H integration on EV adoption. *Appl. Energy* **319**, 119265 (2022).
53. Esmaili, M., Shafiee, H. & Aghaei, J. Range anxiety of electric vehicles in energy management of microgrids with controllable loads. *J. Energy Storage* **20**, 57–66 (2018).
54. Wang, D., Coignard, J., Zeng, T., Zhang, C. & Saxena, S. Quantifying electric vehicle battery degradation from driving vs. vehicle-to-grid services. *J. Power Sources* **332**, 193–203 (2016).
55. Gong, J. et al. Quantifying the impact of V2X operation on electric vehicle battery degradation: an experimental evaluation. *ETransportation* **20**, 100316 (2024).
56. Le, L. B. Building energy management and Electric Vehicle charging considering battery degradation and random vehicles' arrivals and departures. *J. Energy Storage* **64**, 107141 (2023).
57. Ebrahimi, M., Rastegar, M., Mohammadi, M., Palomino, A. & Parvania, M. Stochastic charging optimization of V2G-capable PEVs: a comprehensive model for battery aging and customer service quality. *IEEE Trans. Transp. Electrif.* **6**, 1026–1034 (2020).
58. Sagaria, S., van der Kam, M. & Boström, T. Vehicle-to-grid impact on battery degradation and estimation of V2G economic compensation. *Appl. Energy* **377**, 124546 (2025).
59. Li, Q. & Vittal, V. Non-iterative enhanced SDP relaxations for optimal scheduling of distributed energy storage in distribution systems. *IEEE Trans. Power Syst.* **32**, 1721–1732 (2016).
60. Yang, S., Gao, H. O. & You, F. Integrated optimization in operations control and systems design for carbon emission reduction in building electrification with distributed energy resources. *Adv. Appl. Energy* **12**, 100144 (2023).
61. Yang, P. & Nehorai, A. Joint optimization of hybrid energy storage and generation capacity with renewable energy. *IEEE Trans. Smart Grid* **5**, 1566–1574 (2014).
62. Bian, H. et al. Research on orderly charge and discharge strategy of EV based on QPSO algorithm. *IEEE Access* **10**, 66430–66448 (2022).
63. Hao, X. et al. A V2G-oriented reinforcement learning framework and empirical study for heterogeneous electric vehicle charging management. *Sustain. Cities Soc.* **89**, 104345 (2023).
64. Maeng, J., Min, D. & Kang, Y. Intelligent charging and discharging of electric vehicles in a vehicle-to-grid system using a reinforcement learning-based approach. *Sustain. Energy, Grids Netw.* **36**, 101224 (2023).
65. Dong, J., Yassine, A., Armitage, A. & Hossain, M. S. Multi-agent reinforcement learning for intelligent V2G integration in future transportation systems. *IEEE Trans. Intell. Transp. Syst.* **24**, 15974–15983 (2023).
66. Wu, C., Han, H., Gao, S. & Liu, Y. Coordinated scheduling for multimicrogrid systems considering mobile energy storage characteristics of electric vehicles. *IEEE Trans. Transp. Electrif.* **9**, 1775–1783 (2022).
67. Orfanoudakis, S., et al. Ev2gym: a flexible v2g simulator for ev smart charging research and benchmarking. *IEEE Trans. Intell. Transp. Syst.***26**, 2410–2421 (2024).
68. Zhang, C., Kitamura, H. & Goto, M. Feasibility of vehicle-to-grid (V2G) implementation in Japan: a regional analysis of the electricity supply and demand adjustment market. *Energy* **311**, 133317 (2024).
69. Xu, Y., Çolak, S., Kara, E. C., Moura, S. J. & González, M. C. Planning for electric vehicle needs by coupling charging profiles with urban mobility. *Nat. Energy* **3**, 484–493 (2018).
70. Qian, T., Fang, M., Hu, Q., Shao, C. & Zheng, J. V2Sim: An Open-Source Microscopic V2G Simulation Platform in Urban Power and Transportation Network. *IEEE Trans. Smart Grid* **16**, 1–1 (2025).
71. Zhang, J. et al. Charging demand prediction in Beijing based on real-world electric vehicle data. *J. Energy Storage* **57**, 106294 (2023).
72. Li, P., Zhang, Y., Zhang, Y. & Zhang, K. Prediction of electric bus energy consumption with stochastic speed profile generation modelling and data driven method based on real-world big data. *Appl. Energy* **298**, 117204 (2021).
73. Li, P., Zhang, Y., Zhang, K. & Jiang, M. The effects of dynamic traffic conditions, route characteristics and environmental conditions on trip-based electricity consumption prediction of electric bus. *Energy* **218**, 119437 (2021).
74. Van Haaren, R. Assessment of electric cars' range requirements and usage patterns based on driving behavior recorded in the National Household Travel Survey of 2009. *Electr. Cars' Range Requir. Usage Patterns* **51**, 53 (2011).
75. Longshine Technology Group Co., L. *Xindiantu - Aggregated charging service platform*, https://www.longshine.com/solutionInfo/81(2024).
76. Huang, W. et al. Capacity optimization of PV and battery storage for EVCS with multi-venues charging behavior difference towards economic targets. *Energy* **313**, 133833 (2024).
77. Feng, J., Cui, C., Zhang, C. & Fan, Z. in *2025 10th Asia Conference on Power and Electrical Engineering (ACPEE)*. 2683–2687 (IEEE, 2025).
78. Wang, Z. *Annual Report on the Big Data of New Energy Vehicle in China* (China Machine Press, 2020).
79. Barthélemy, M. Spatial networks. *Phys. Rep.* **499**, 1–101 (2011).
80. Antoniadou-Plytaria, K., Steen, D., Carlson, O. & Ghazvini, M. A. F. Market-based energy management model of a building microgrid considering battery degradation. *IEEE Trans. Smart Grid* **12**, 1794–1804 (2020).
81. Nunna, H. K., Battula, S., Doolla, S. & Srinivasan, D. Energy management in smart distribution systems with vehicle-to-grid integrated microgrids. *IEEE Trans. Smart Grid* **9**, 4004–4016 (2016).
82. Li, K. Unlocking vehicle-to-grid potential of load shifting in China's megacities considering comprehensive real-world behaviors: code instruction. *CodeOcean* https://doi.org/10.24433/CO.2863234.v1 (2025).
83. Li, K. Unlocking vehicle-to-grid potential of load shifting in China's megacities considering comprehensive real-world behaviors: Source Data. figshare. Dataset. https://doi.org/10.6084/m9.figshare.27950028 (2025).

Acknowledgements

This research was supported by Shenzhen Science and Technology Program KCXST20221021111608020 (H. Qi, Y. Zhang).

Author contributions

K. Li (李楷三): Methodology, software, validation, formal analysis, data curation, writing—original draft, writing—review and editing, visualization. X. Li (李欣欣): Methodology, software, investigation, writing—original draft. Z. Xiong (熊祖逊): Methodology, software, writing—review and editing. S. Tao (陶晟宇): Writing—review and editing. G. Zhao (赵谷橙): Visualization. Y. Jiang (江亿): Conceptualization, project administration. H. Qi (齐贺): Conceptualization, project administration. Y. Zhang (张一): Conceptualization, resources, writing—original draft, writing—review & editing, supervision, project administration, funding acquisition.

Competing interests

The authors declare no competing interests.

Additional information

Supplementary information The online version contains supplementary material available at https://doi.org/10.1038/s41467-025-65073-8.

Correspondence and requests for materials should be addressed to Yi Zhang.

Peer review information *Nature Communications* thanks the anonymous, reviewer(s) for their contribution to the peer review of this work. A peer review file is available.